

Kilonova and Optical Afterglow from Binary Neutron Star Mergers. II. Optimal Search Strategy for Serendipitous Observations and Target-of-opportunity Observations of Gravitational-wave Triggers

JIN-PING ZHU ¹, SHICHAO WU ^{2,3}, YUAN-PEI YANG ⁴, CHANG LIU ^{1,5}, BING ZHANG ^{6,7}, HAO-RAN SONG ⁸,
HE GAO ⁸, ZHOUJIAN CAO ⁸, YUN-WEI YU ⁹, YACHENG KANG ^{1,5} AND LIJING SHAO ^{5,10}

¹Department of Astronomy, School of Physics, Peking University, Beijing 100871, China; zhujp@pku.edu.cn

²Max-Planck-Institut für Gravitationsphysik (Albert-Einstein-Institut), D-30167 Hannover, Germany; shichao.wu@aei.mpg.de

³Leibniz Universität Hannover, D-30167 Hannover, Germany

⁴South-Western Institute for Astronomy Research, Yunnan University, Kunming, Yunnan, People's Republic of China; ypyang@ynu.edu.cn

⁵Kavli Institute for Astronomy and Astrophysics, Peking University, Beijing 100871, China

⁶Nevada Center for Astrophysics, University of Nevada, Las Vegas, NV 89154, USA; bing.zhang@unlv.edu

⁷Department of Physics and Astronomy, University of Nevada, Las Vegas, NV 89154, USA

⁸Department of Astronomy, Beijing Normal University, Beijing 100875, China

⁹Institute of Astrophysics, Central China Normal University, Wuhan 430079, China

¹⁰National Astronomical Observatories, Chinese Academy of Sciences, Beijing 100012, China

ABSTRACT

In the second work of this series, we explore the optimal search strategy for serendipitous and gravitational-wave-triggered target-of-opportunity (ToO) observations of kilonovae and optical short-duration gamma-ray burst (sGRB) afterglows from binary neutron star (BNS) mergers, assuming that cosmological kilonovae are AT2017gfo-like (but with viewing-angle dependence) and that the properties of afterglows are consistent with those of cosmological sGRB afterglows. A one-day cadence serendipitous search strategy with an exposure time of ~ 30 s can always achieve an optimal search strategy of kilonovae and afterglows for various survey projects. We show that the optimal detection rates of the kilonovae (afterglows) are $\sim 0.3/0.6/1/20 \text{ yr}^{-1}$ ($\sim 50/60/100/800 \text{ yr}^{-1}$) for ZTF/Mephisto/WFST/LSST, respectively. A better search strategy for SiTian than the current design is to increase the exposure time. In principle, a fully built SiTian can detect $\sim 7(2000) \text{ yr}^{-1}$ kilonovae (afterglows). Population properties of electromagnetic (EM) signals detected via the serendipitous observations are studied in detail. For ToO observations, we predict that one can detect $\sim 11 \text{ yr}^{-1}$ BNS gravitational wave (GW) events during the fourth observing run (O4) by considering an exact duty cycle of the third observing run. The median GW sky localization area is expected to be $\sim 10 \text{ deg}^2$ for detectable BNS GW events. For O4, we predict that ZTF/Mephisto/WFST/LSST can detect $\sim 5/4/3/3$ kilonovae ($\sim 1/1/1/1$ afterglows) per year, respectively. The GW detection rates, GW population properties, GW sky localizations, and optimistic ToO detection rates of detectable EM counterparts for BNS GW events at the Advanced Plus, LIGO Voyager and ET&CE eras are detailedly simulated in this paper.

Keywords: Gravitational waves (678), Neutron stars (1108), Gamma-ray bursts (629)

1. INTRODUCTION

Kilonovae (Li & Paczyński 1998; Metzger et al. 2010) and short-duration gamma-ray bursts (sGRB; Paczynski 1986, 1991; Eichler et al. 1989; Narayan et al. 1992; Zhang 2018) have long been thought to originate from binary neutron star (BNS) and neutron star–black hole (NSBH) mergers. The interaction of the sGRB relativistic jets with the surrounding interstellar medium would

produce bright afterglow emissions from X-ray to radio¹

¹ If BNS and NSBH mergers occur in active galactic nucleus (e.g., Cheng & Wang 1999; McKernan et al. 2020) accretion disks, sGRB relativistic jets would always be choked and kilonova emissions would be outshone by the disk emission (Zhu et al. 2021d; Perna et al. 2021). The choked jets and subsequent jet-cocoon and ejecta shock breakouts can generate high-energy neutrinos which may significantly contribute diffuse neutrino background (Zhu et al. 2021a,b).

(Rees & Meszaros 1992; Meszaros & Rees 1993; Paczynski & Rhoads 1993; Mészáros & Rees 1997; Sari et al. 1998; Gao et al. 2013b).

On 2017 August 17, the first BNS gravitational wave (GW) event, i.e., GW170817, was detected by the Advanced Laser Interferometer Gravitational Wave Observatory (LIGO; Harry & LIGO Scientific Collaboration 2010; LIGO Scientific Collaboration et al. 2015) and the Advanced Virgo (Acernese et al. 2015) detectors (Abbott et al. 2017a). This BNS GW event has been subsequently confirmed in connection with an sGRB (GRB170817A; Abbott et al. 2017b; Goldstein et al. 2017; Savchenko et al. 2017; Zhang et al. 2018a), an ultraviolet–optical–infrared kilonova (AT2017gfo; Abbott et al. 2017c; Andreoni et al. 2017; Arcavi et al. 2017; Chornock et al. 2017; Coulter et al. 2017; Covino et al. 2017; Cowperthwaite et al. 2017; Díaz et al. 2017; Drout et al. 2017; Evans et al. 2017; Hu et al. 2017; Kasliwal et al. 2017; Kilpatrick et al. 2017; Lipunov et al. 2017; McCully et al. 2017; Nicholl et al. 2017; Pian et al. 2017; Shappee et al. 2017; Smartt et al. 2017; Soares-Santos et al. 2017; Tanvir et al. 2017; Utsumi et al. 2017; Valenti et al. 2017; Villar et al. 2017) and a broadband off-axis jet afterglow (Alexander et al. 2017; Haggard et al. 2017; Hallinan et al. 2017; Margutti et al. 2017; Troja et al. 2017, 2018, 2020; D’Avanzo et al. 2018; Dobie et al. 2018; Lazzati et al. 2018; Lyman et al. 2018; Xie et al. 2018; Piro et al. 2019; Ghirlanda et al. 2019). The multi-messenger observations of this BNS merger provided smoking-gun evidence for the long-hypothesized origin of sGRBs and kilonovae, and heralded the advent of the GW-led astronomy era.

To date, except for AT2017gfo, other kilonova candidates were all detected in superposition with decaying sGRB afterglows (e.g., Berger et al. 2013; Tanvir et al. 2013; Fan et al. 2013; Gao et al. 2015, 2017; Jin et al. 2015, 2016, 2020; Yang et al. 2015; Gompertz et al. 2018; Ascenzi et al. 2019; Rossi et al. 2020; Ma et al. 2021; Fong et al. 2021; Wu et al. 2021; Yuan et al. 2021). Interestingly, a bright kilonova candidate was found to be associated with a long-duration GRB 211211A in recent (e.g., Rastinejad et al. 2022; Troja et al. 2022; Yang et al. 2022b; Zhu et al. 2022a). One possible reason almost all kilonova candidates were detected in GRB afterglows is that most BNS and NSBH mergers are far away from us. Their associated kilonova signals may be too faint to be directly detected by present survey projects. However, thanks to the beaming effect of relativistic jets, in Paper I of this series (Zhu et al. 2022c), we have shown that a large fraction of cosmological afterglows could be much brighter than the associated kilonovae if the jets move towards or close to the line of sight. Bright

afterglow emissions would help us detect potential associated kilonova emissions. On the other hand, a too bright afterglow would also affect on the detectability of the associated kilonova.

Catching more kilonovae and afterglows by current and future survey projects would be helpful for expanding our knowledge about the population properties of these events. Kasliwal et al. (2020); Mohite et al. (2021) constrained the population properties of kilonovae based on the non-detection of GW-triggered follow-up observations during O3. Although the properties of kilonova and afterglow emissions from BNS and NSBH mergers can be reasonably well predicted, their low luminosities and fast evolution nature compared with supernova emission make it difficult to detect them using the traditional time-domain survey projects. Several works in the literature have studied the detection rates and search strategy for kilonovae by serendipitous observations (e.g., Metzger & Berger 2012; Coughlin et al. 2017, 2020a; Rosswog et al. 2017; Scolnic et al. 2018; Setzer et al. 2019; Sagués Carracedo et al. 2021; Zhu et al. 2021d; Andreoni et al. 2021a; Almualla et al. 2021; Chase et al. 2021). Because afterglow emission could significantly affect the observation of a fraction of kilonova events, one cannot ignore the effect of afterglow emission when considering the search strategy and detectability of kilonova emission. In the second work of this series, we will perform a detailed study on optimizing serendipitous detections of both kilonovae and optical afterglows with different cadences, filters, and exposure times for several present and future survey projects. The survey projects we consider in this work include the Zwicky Transient Facility (ZTF; Bellm et al. 2019; Masci et al. 2019), the Multi-channel Photometric Survey Telescope² (Mephisto; Er et al. 2022, in preparation), the Wide Field Survey Telescope (WFST; et al. Kong et al. 2022, in preparation), the Large Synoptic Survey Telescope (LSST; LSST Science Collaboration et al. 2009), and the SiTian Projects (SiTian; Liu et al. 2021). We note that (1) NSBH mergers may have a lower event rate density; (2) NSBH kilonovae may be dimmer than BNS kilonovae (e.g., Zhu et al. 2020); (3) most NSBH mergers in the universe are likely plunging events (e.g., Abbott et al. 2021a; Zappa et al. 2019; Drozda et al. 2020; Zhu et al. 2022b, 2021c; Broekgaarden et al. 2021; Hu et al. 2022). As a result, the detection rates of kilonova and afterglow emissions from NSBH mergers should be much lower than those from BNS mergers (Zhu et al. 2021e).

² <http://www.mephisto.ynu.edu.cn/site/>

In the following calculations, we only consider sGRB, kilonova and afterglow emissions from BNS mergers.

Furthermore, with the upgrade and iteration of GW observatories, numerous BNS mergers from the distant universe will be discovered. Future foreseeable GW observations will give a better constraint on the localization for a fraction of BNS GW events, which will benefit the search for associated electromagnetic (EM) counterparts. For example, some GW sources will be localized to $\sim 10 \text{ deg}^2$ by the network including the Advanced LIGO, Advanced Virgo, and KAGRA GW detectors (Abbott et al. 2020a; Frostig et al. 2021). Therefore, taking advantage of target-of-opportunity (ToO) follow-up observations of GW triggers will greatly improve the search efficiency of kilonovae and afterglows, although Petrov et al. (2022) recently suggested that the previous expectations for the GW sky localization may be too optimistic. The kilonova follow-up campaigns by specific survey projects, e.g., ZTF, LSST, and the Wide-Field Infrared Transient Explorer, for GW BNS mergers in the near GW era have been simulated recently (Sagués Carracedo et al. 2021; Cowperthwaite et al. 2019; Frostig et al. 2021). In this paper, we present detailed calculations of the BNS detectability by the GW detectors in the next 15 yr and the associated EM detectability for GW-triggered ToO observations.

The paper is organized as follows. The physical models are briefly presented in Section 2. More details of our models have been presented in Paper I. The search strategy and detectability of kilonova and afterglow emissions for time-domain survey observations are studied in Section 3. We also perform some calculations for the EM detection rates by some specific survey projects. In Section 4, we simulate the GW detection and subsequent detectability of EM ToO follow up observations for networks of 2nd-, 2.5th-, and 3rd-generation GW detectors. Finally, we summarize our conclusions and present some discussions in Section 5. A standard Λ CDM cosmology with $H_0 = 67.8 \text{ km s}^{-1} \text{ Mpc}^{-1}$, $\Omega_\Lambda = 0.692$, and $\Omega_m = 0.308$ (Planck Collaboration et al. 2016) is applied in this paper.

2. MODELLING

2.1. Redshift Distribution and EM Properties of Simulated BNS Populations

The total number of BNS mergers in the universe can be estimated as (e.g., Sun et al. 2015)

$$\dot{N}_{\text{BNS}} \approx \int_0^{z_{\text{max}}} \frac{\dot{\rho}_{0,\text{BNS}} f(z)}{1+z} \frac{dV(z)}{dz} dz, \quad (1)$$

where $\dot{\rho}_{0,\text{BNS}}$ is the local BNS event rate density, $f(z)$ is the dimensionless redshift distribution factor, and z_{max}

is the maximum redshift for BNS mergers. The comoving volume element $dV(z)/dz$ in Equation (1) is

$$\frac{dV}{dz} = \frac{c}{H_0} \frac{4\pi D_L^2}{(1+z)^2 \sqrt{\Omega_\Lambda + \Omega_m(1+z)^3}}, \quad (2)$$

where c is the speed of light and D_L is the luminosity distance, which is expressed as

$$D_L = (1+z) \frac{c}{H_0} \int_0^z \frac{dz}{\sqrt{\Omega_\Lambda + \Omega_m(1+z)^3}} \quad (3)$$

Recently, Abbott et al. (2021b) estimated the local BNS event rate density as $\dot{\rho}_{0,\text{BNS}} = 320_{-240}^{+490} \text{ Gpc}^{-3} \text{ yr}^{-1}$ based on the GW observations during the first half of the third observing (O3) run (see Mandel & Broekgaarden 2021, for a review of $\dot{\rho}_{0,\text{BNS}}$). Hereafter, if not otherwise specified, $\dot{\rho}_{0,\text{BNS}}$ used in our calculations are simply set as the median value of the GW constraint by the LIGO/Virgo Collaboration (LVC), i.e., $\dot{\rho}_{0,\text{BNS}} \simeq 320 \text{ Gpc}^{-3} \text{ yr}^{-1}$.

BNS mergers can be thought as occurring with a delay timescale with respect to the star formation history. The Gaussian delay model (Virgili et al. 2011), log-normal delay model (Nakar et al. 2006; Wanderman & Piran 2015), and power-law delay model (Virgili et al. 2011; Hao & Yuan 2013; D’Avanzo et al. 2014) are main types of delay time distributions. Sun et al. (2015) suggested that the power-law delay model leads to a wider redshift distribution of BNS merger than other two models, while recent observations on sGRBs by Zevin et al. (2022); Fong et al. (2022); O’Connor et al. (2022); Nugent et al. (2022) supported power-law delay more. Although many debates, for simplicity, we only adopt the log-normal delay model as our merger delay model and the analytical fitting expression of $f(z)$ is presented as Equation (A8) in Zhu et al. (2021e). With known redshift distribution $f(z)$, we randomly simulate a group of $n_{\text{sim}} = 5 \times 10^6$ BNS events in the universe based on Equation (1). For each BNS event, we then generate its EM emissions. We briefly assume that all of BNS events in the universe would only power three main types of EM signals, i.e. the jet afterglow, the kilonova, and the sGRB. We assume that cosmological kilonovae are AT2017gfo-like with the consideration of the viewing-angle effect, while the properties of afterglows are consistent with those of cosmological sGRB afterglows. The modeling details of redshift distribution, jet afterglow and kilonova emissions of BNS mergers has been presented in Paper I. Our viewing-angle-dependent semi-analytical model of sGRB emission follows Song et al. (2019) and Yu et al. (2021). The signature of sGRBs depends on the on-axis equivalent isotropic energy E_0 , the core half-opening angle θ_c , and the latitudinal view-

ing angle θ_{view} , while the afterglow emission has a dependence on four additional parameters, i.e. number density of interstellar medium n , power-law index of the electron distribution p , fractions of shock energy distributed in electrons, ε_e , and in magnetic fields, ε_B . Furthermore, the kilonova emission is only determined by θ_{view} . According to the distributions of above parameters as described in Paper I in detail, one can randomly generate the EM emission components for each simulated BNS event.

2.2. Classification of Detectable EM Counterparts

We divide the detectable events into two main groups based on the relative brightness of the detected kilonova and afterglow. If the peak kilonova flux is larger than five times of the afterglow flux, i.e., $F_{\nu,\text{KN}}(t_{\text{KN,p}}) > 5F_{\nu,\text{AG}}(t_{\text{KN,p}})$, where $t_{\text{KN,p}}$ is the peak time of the kilonova, we qualify these events into “kilonova-dominated sample”. For such events, kilonova emission at the peak time would be at least two magnitudes brighter than that of the associated afterglow emission, so that this requirement can guarantee a clear kilonova signal for observers. For on-axis or near-on-axis afterglows, some bright kilonovae can appear detectable as an excess flux compared to the afterglow power-law decay, which are also defined as kilonova-dominated events. Other events are classified as “afterglow-dominated sample”, since the observed kilonova signals of these events may be ambiguous. In Paper I, we have shown that $\sim 50\%$ on-axis and nearly-on-axis afterglows are brighter than the associated kilonovae at the peak time. Thus, most of them would be afterglow-dominated. Only at large viewing angles with $\sin\theta_v \gtrsim 0.20$, the EM signals of most BNS mergers would be kilonova-dominated and some off-axis afterglows may emerge at $\sim 5 - 10$ day after the mergers.

Some optically-discovered EM counterparts of BNS mergers could be associated with sGRB observations. For the GW-triggered ToO searches, the observations of sGRBs can cooperate on the constraint on the sky location for BNS GW alerts, which would help us find the EM counterparts. On the basis of whether or not an sGRB is detected, we can further divide each sample into two subsamples, i.e., (1) kilonova-dominated sample: kilonova with (w/) sGRB and kilonova without (w/o) sGRB; (2) afterglow-dominated sample: afterglow w/ sGRB and afterglow w/o sGRB. Furthermore, a fraction of BNS mergers may only be detected in the γ -ray band without any detection of an associated optical afterglow or kilonova. Thus, we totally define five subsamples for the EM counterparts of BNS mergers (see Table 1).

SGRBs are believed to be triggered if $F_\gamma > F_{\gamma,\text{limit}}$, where F_γ is the γ -band flux for each BNS GW event (see Song et al. 2019; Yu et al. 2021, for the details of sGRB model) and $F_{\gamma,\text{limit}}$ is the effective sensitivity limit for various γ -ray detectors. Many GRB detectors with quick response and wide field of view, e.g., Swift (Gehrels et al. 2004), AstroSAT (Singh et al. 2014), Fermi (Meegan et al. 2009), and GECAM (Zhang et al. 2018b; Song et al. 2019), will work during O4. In our calculations, we simply set $F_{\gamma,\text{limit}} \sim 2 \times 10^{-7} \text{ erg s}^{-1}$ in 50 – 300 keV which is the effective sensitivity limit of Fermi-GBM (Meegan et al. 2009) and GECAM (Zhang et al. 2018b; Song et al. 2019), in view of that Fermi-GBM and GECAM can nearly achieve an all-sky coverage to detect GRB events³.

3. DETECTABILITY FOR SERENDIPITOUS SEARCHES

In this Section, we will introduce the method for the calculations of the EM detection rate via the serendipitous observations, investigate on the optimal search strategy, and show our simulated optically-discovered detection rates of the kilonova-dominated and afterglow-dominated events for some specific survey projects. By considering the observations of sGRBs, the population properties for detectable EM events via the serendipitous searches are detailedly discussed in the following.

3.1. Method

Following Zhu et al. (2021e), we adopt a method of probabilistic statistical analysis to estimate the EM detection rate for BNS mergers. The probability that a single simulated event can be detected could be considered as the ratio of survey area within the time duration (Δt) that the brightness of the associated EM signal is above the limiting magnitude (m_{limit}) to the area of the celestial sphere ($\Omega_{\text{sph}} = 41252.96 \text{ deg}^2$). The maximum probability for a source to be detected is $\Omega_{\text{FoV}} \dot{t}_{\text{ope}} \Delta t / \Omega_{\text{sph}} (n_{\text{exp}} t_{\text{exp}} + t_{\text{oth}})$, where Ω_{FoV} is the field of view (FoV) for the specific survey project, \dot{t}_{ope} is the average operation time per day, n_{exp} is defined as the exposure number for each visit, t_{exp} is the exposure time, and t_{other} is other time spent for each visit. However, high-cadence observations would restrict the sur-

³ Compared with Fermi-GBM and GECAM, Swift-BAT (Gehrels et al. 2004; Lien et al. 2014) has a much lower sensitivity of $F_{\gamma,\text{limit}} \sim 1 \times 10^{-8} \text{ erg s}^{-1}$ in 15 – 150 keV. However, unlike Fermi-GBM and GECAM that can nearly achieve an all-sky coverage, the Swift-BAT’s FoV is $\sim 1.4 \text{ sr}$. It is expected that the number of events with γ -ray triggers by Swift/BAT could be even lower than that by Fermi-GBM and GECAM due to its limited FoV (e.g., Song et al. 2019).

Table 1. Sample for EM counterparts of BNS mergers

Sample	sGRB	kilonova-dominated	afterglow-dominated
kilonova w/ sGRB	✓	✓	✗
kilonova w/o sGRB	✗	✓	✗
afterglow w/ sGRB	✓	✗	✓
afterglow w/o sGRB	✗	✗	✓
sGRB only	✓	✗	✗

vey area, which means that the probability of a source being detected by the high-cadence search would be a constant, i.e., $\Omega_{\text{FoV}} \dot{t}_{\text{ope}} t_{\text{cad}} / \Omega_{\text{sph}} (n_{\text{exp}} t_{\text{exp}} + t_{\text{oth}})$, where the cadence time t_{cad} defined as the interval between consecutive observations of the same sky area by a telescope. Furthermore, the event should appear in the sky coverage of the survey telescope that one can have a chance to discover it. Thus, we simply set an upper limit on the probability for a source that can be detected, which is expressed as $\Omega_{\text{cov}} / \Omega_{\text{sph}}$ with Ω_{cov} being the detectable sky coverage for a specific survey project. By counting the detection probabilities of all simulated events, one can write the EM detection rate for the serendipitous observations as

$$\dot{N}_{\text{EM}} \approx \frac{\dot{N}_{\text{BNS}}}{n_{\text{sim}}} \sum_{i=1}^{n_{\text{sim}}} \min \left[\frac{\Omega_{\text{cov}}}{\Omega_{\text{sph}}}, \frac{\Omega_{\text{FoV}} \dot{t}_{\text{ope}} \min(t_{\text{cad}}, \Delta t_i)}{\Omega_{\text{sph}} (n_{\text{exp}} t_{\text{exp}} + t_{\text{oth}})} \right], \quad (4)$$

We roughly assume that the average operation time per day is $\dot{t}_{\text{ope}} \approx 6 \text{ hr day}^{-1}$ for all survey projects except for SiTian. The time spent for each visit t_{oth} is dependent on the technical performance of specific survey project and different search strategy. Because t_{oth} is uncertain, we set it as a constant for each survey project, i.e., $t_{\text{oth}} = 15 \text{ s}$.

In order to reject the supernova background and other rapid-evolving transients, in [Paper I](#), we showed that one can use the unique color evolution of kilonovae and afterglows to identify them among the observed transients. We require that the judgement condition for the detection of the kilonova and/or afterglow by a serendipitous search is that “two different exposure filters have at least two detection epochs”. It would be $n_{\text{exp}} = 1$ for Mephisto and SiTian since these two survey projects

can achieve simultaneous imaging in three bands,⁴ while $n_{\text{exp}} = 2$ for ZTF, WFST, and LSST.

The values of some technical parameters, including the expected limiting magnitude which is a logarithmic function of exposure time in each band, FoV, detectable sky coverage, for the survey telescopes we considered are presented in [Table 2](#). As examples, we also list g -band limiting magnitudes $m_{g,\text{limit}}$ with different exposure times of $t_{\text{exp}} = 30, 180, 300 \text{ s}$ for these survey telescopes in [Table 2](#). Thus, survey telescopes with aperture that smaller than ZTF and SiTian can have a limiting magnitude of $m_{\text{limit}} \lesssim 20 \text{ mag}$. The detection depth of ZTF and SiTian locates in a range of $20 \text{ mag} \lesssim m_{\text{limit}} \lesssim 22 \text{ mag}$. It expects that $22 \text{ mag} \lesssim m_{\text{limit}} \lesssim 24 \text{ mag}$ applies to Mephisto and WFST. $24 \lesssim m_{\text{limit}} \lesssim 26 \text{ mag}$ can be only achieved by LSST.

3.2. Δt_{EM} and Cadence Time Selection

As listed in [Table 3](#), we show the 90% credible regions of two timescales, i.e., Δt_{KN} and Δt_{AG} , with different filters and different limiting magnitudes. These two parameters are respectively defined as the timescales during which the brightness of the associated kilonova and afterglow is above the limiting magnitude in different bands. Because gri bands are the common filters used by various survey projects, we only show the probability density functions of Δt_{KN} and Δt_{AG} with different searching magnitudes in these three bands in [Figure 1](#).

As shown in [Table 3](#), for a limiting magnitude of $m_{\text{limit}} \leq 19 \text{ mag}$, the values of Δt_{KN} may be imprecise, due to the limited amount of the available data. For $m_{\text{limit}} \geq 20 \text{ mag}$, one can see that the median value of Δt_{KN} is referred to lie $\sim 0.6 - 1.4 \text{ day}$ in optical

⁴ The optical system of Mephisto consists of a modified Ritchey-Chrétien design with three refractive correctors and three cubes for beam splitting so that it can be capable of simultaneously imaging the same patch of sky in three bands (Er et al. 2022, in preparation). SiTian is composed of a number of “units” which is made of three 1-m-class Schmidt telescopes (see [Section 3.4](#) for more details). Both of them can achieve simultaneous imaging in three bands.

Table 2. Summary Technical Information for Each Survey

Telescope	$m_{\text{limit}} = a \times t_{\text{exp}}^b$						t_{exp}/s	$m_{g,\text{limit}}/\text{mag}$	FoV/deg ²	Sky Coverage/deg ²	Reference
ZTF	<i>g</i>		<i>r</i>		<i>i</i>		30	20.3			
	18.62		18.37		17.91		180	21.3	47.7	30,000	(1)
	0.026		0.026		0.027		300	21.6			
Mephisto	<i>u</i>	<i>v</i>	<i>g</i>	<i>r</i>	<i>i</i>	<i>z</i>	30	22.4			
	18.45	18.54	19.91	19.91	19.68	18.71	180	23.8	3.14	26,000	(2)
	0.043	0.042	0.034	0.032	0.030	0.033	300	24.2			
WFST	<i>u</i>	<i>g</i>	<i>r</i>	<i>i</i>	<i>z</i>	<i>w</i>	30	23.0			
	20.70	21.33	21.13	20.46	19.41	21.33	180	23.9	6.55	20,000	(3)
	0.022	0.022	0.022	0.023	0.024	0.022	300	24.2			
LSST	<i>u</i>	<i>g</i>	<i>r</i>	<i>i</i>	<i>z</i>	<i>y</i>	30	25.1			
	22.03	23.60	22.54	21.73	21.83	21.68	180	25.9	9.6	20,000	(4)
	0.025	0.018	0.023	0.030	0.031	0.032	300	26.2			
SiTian*	<i>g</i>		<i>r</i>		<i>i</i>		30	20.3			
	18.62		18.37		17.91		180	21.3	600	30,000	(5)
	0.026		0.026		0.027		300	21.6			

NOTE—The columns are [1] the survey project; [2] the search limiting magnitude m_{limit} as a logarithmic function of exposure time t_{exp} in different bands for specific survey project (parameter a and b are respectively the values at the second and third sub-rows of each row); [3] exposure time t_{exp} ; [4] g -band limiting magnitude $m_{g,\text{limit}}$ corresponding to different exposure times; [5] field of view Ω_{FoV} ; [6] detectable sky coverage Ω_{cov} ; [7] references.

Reference: (1) [Bellm et al. \(2019\)](#); [Masci et al. \(2019\)](#); (2) [Er et al. \(2022\)](#), in preparation; [Lei et al. \(2021\)](#) (3) [Kong et al. \(2022\)](#), in preparation; [Shi et al. \(2018\)](#) (4) [LSST Science Collaboration et al. \(2009\)](#); (5) [Liu et al. \(2021\)](#).

* The technical specification of the limiting magnitude in the g -band stacked images for SiTian is similar to that for ZTF ([Liu et al. 2021](#)). SiTian would simultaneously observe the same visit in three different filters (u , g , i). Due to the lack of the technical information in u and i band of SiTian, we simply use the technical information of ZTF in gri bands to calculate the EM detection rates by SiTian.

and $\sim 1.4 - 2.1$ day in infrared, which may be uncorrelated with the limiting magnitude m_{limit} . If the observer wants to achieve at least two detection epochs for at least 50% of the observable kilonova signals, the cadence time t_{cad} should be less than half of the median value of Δt_{KN} . This means t_{cad} should be $t_{\text{cad}} \lesssim 0.3 - 0.7$ day if one uses an optical band to search for kilonovae and $t_{\text{cad}} \lesssim 0.7 - 1.0$ day by an infrared band for all survey projects.

Unlike Δt_{KN} , there exists a positive correlation between Δt_{AG} and m_{limit} listed in Table 3. The median value of Δt_{KN} would be always larger than Δt_{AG} if $m_{\text{limit}} \lesssim 24$ mag. Thus, LSST, which has a limiting magnitude of $m_{\text{limit}} \gtrsim 24$ mag, can find $\gtrsim 50\%$ detectable afterglows brighter than the searching limiting magnitude by adopting a cadence to search for kilonovae. As shown in Figure 1, the probability density function of Δt_{AG} is significantly higher than that of Δt_{KN} , especially for searching with a relatively shallow limiting magnitude in a bluer filter band. Thus, it may be easier

to discover optical afterglows by adopting the cadence of searching for kilonovae.

3.3. Optimal Search Strategy

We respectively show the detection rates of kilonova-dominated and afterglow-dominated sample for ZTF, Mephisto, WFST, and LSST in Figure 2 and Figure 3, by considering exposure time from 30s to 300s and five different cadence timescales $t_{\text{cad}} = 0.5$ hr, 1 hr, 3 hr, 1 day, and 2 day. The results shown in Figure 2 and Figure 3 are only considered in gri bands since these three bands are commonly used for these survey telescopes. Because SiTian is an integrated network of dozens of survey and follow-up telescopes, its survey strategy should have a large difference with that of other survey projects. We will give an separate calculation of EM detection rates for SiTian in Section 3.4.

As shown in Figure 2, for each survey project, the difference of the detection rate for kilonova-dominated events between different bands seems very small, which is a factor of the order of unity. For the cadence choice,

Table 3. Time during which the brightness of EM counterpart is above the limiting magnitude

Filter	Parameter	$m_{\text{limit}} = 18 \text{ mag}$	19 mag	20 mag	21 mag	22 mag	23 mag	24 mag	25 mag	26 mag
u	Δt_{KN}	–	$0.67^{+0}_{-0.67}$	$0.65^{+0.77}_{-0.65}$	$0.82^{+0.63}_{-0.72}$	$0.8^{+1.1}_{-0.6}$	$0.7^{+1.4}_{-0.6}$	$0.7^{+1.3}_{-0.5}$	$0.7^{+1.2}_{-0.6}$	$0.8^{+1.2}_{-0.6}$
	Δt_{AG}	$0.12^{+0.55}_{-0.11}$	$0.14^{+0.68}_{-0.12}$	$0.18^{+0.91}_{-0.16}$	$0.2^{+1.3}_{-0.2}$	$0.3^{+1.9}_{-0.3}$	$0.4^{+3.0}_{-0.4}$	$0.6^{+4.7}_{-0.5}$	$0.9^{+7.5}_{-0.8}$	2^{+12}_{-1}
g	Δt_{KN}	$0.83^{+0}_{-0.83}$	$0.7^{+1.1}_{-0.7}$	$1.3^{+0.8}_{-1.2}$	$1.2^{+1.4}_{-1.0}$	$1.2^{+1.9}_{-0.9}$	$1.1^{+1.7}_{-0.8}$	$1.0^{+1.7}_{-0.7}$	$0.9^{+1.8}_{-0.7}$	$0.9^{+1.9}_{-0.7}$
	Δt_{AG}	$0.12^{+0.58}_{-0.11}$	$0.15^{+0.73}_{-0.13}$	$0.19^{+0.97}_{-0.17}$	$0.2^{+1.4}_{-0.2}$	$0.3^{+2.1}_{-0.3}$	$0.4^{+3.3}_{-0.4}$	$0.6^{+5.2}_{-0.5}$	$1.0^{+8.1}_{-0.9}$	2^{+13}_{-2}
v	Δt_{KN}	$1.4^{+0}_{-1.4}$	$0.7^{+1.1}_{-0.6}$	$1.1^{+1.5}_{-0.8}$	$1.0^{+2.4}_{-0.8}$	$1.1^{+2.3}_{-0.7}$	$1.0^{+2.0}_{-0.8}$	$1.1^{+1.9}_{-0.8}$	$1.2^{+2.0}_{-0.9}$	$1.3^{+1.9}_{-0.7}$
	Δt_{AG}	$0.13^{+0.60}_{-0.12}$	$0.15^{+0.77}_{-0.13}$	$0.2^{+1.0}_{-0.2}$	$0.2^{+1.5}_{-0.2}$	$0.3^{+2.2}_{-0.3}$	$0.4^{+3.4}_{-0.4}$	$0.6^{+5.4}_{-0.6}$	$1.0^{+8.6}_{-1.0}$	2^{+13}_{-2}
w	Δt_{KN}	$0.5^{+1.1}_{-0.5}$	$0.89^{+0.88}_{-0.60}$	$1.2^{+1.6}_{-0.9}$	$1.2^{+2.3}_{-0.8}$	$1.2^{+2.3}_{-0.8}$	$1.1^{+2.3}_{-0.8}$	$1.1^{+2.2}_{-0.8}$	$1.2^{+2.1}_{-0.8}$	$1.3^{+2.0}_{-1.0}$
	Δt_{AG}	$0.13^{+0.61}_{-0.12}$	$0.15^{+0.78}_{-0.13}$	$0.2^{+1.0}_{-0.2}$	$0.2^{+1.5}_{-0.2}$	$0.3^{+2.2}_{-0.3}$	$0.4^{+3.5}_{-0.4}$	$0.6^{+5.5}_{-0.6}$	$1.1^{+8.7}_{-1.0}$	2^{+14}_{-2}
r	Δt_{KN}	$0.7^{+1.0}_{-0.7}$	$1.07^{+0.88}_{-0.69}$	$1.3^{+1.7}_{-1.0}$	$1.2^{+2.5}_{-0.8}$	$1.1^{+2.4}_{-0.8}$	$1.3^{+2.1}_{-0.9}$	$1.3^{+2.2}_{-0.9}$	$1.2^{+2.4}_{-0.9}$	$1.3^{+2.4}_{-0.9}$
	Δt_{AG}	$0.13^{+0.63}_{-0.12}$	$0.15^{+0.79}_{-0.13}$	$0.2^{+1.1}_{-0.2}$	$0.3^{+1.5}_{-0.2}$	$0.3^{+2.3}_{-0.3}$	$0.4^{+3.6}_{-0.4}$	$0.7^{+5.6}_{-0.6}$	$1.1^{+8.9}_{-1.0}$	2^{+14}_{-2}
i	Δt_{KN}	$0.7^{+1.9}_{-0.7}$	$1.3^{+1.3}_{-0.7}$	$1.5^{+2.2}_{-1.3}$	$1.4^{+3.1}_{-0.9}$	$1.3^{+2.6}_{-1.0}$	$1.3^{+2.4}_{-1.0}$	$1.4^{+2.4}_{-0.9}$	$1.4^{+2.5}_{-1.0}$	$1.7^{+2.6}_{-1.2}$
	Δt_{AG}	$0.13^{+0.67}_{-0.12}$	$0.16^{+0.84}_{-0.14}$	$0.2^{+1.1}_{-0.2}$	$0.3^{+1.6}_{-0.2}$	$0.3^{+2.4}_{-0.3}$	$0.5^{+3.8}_{-0.4}$	$0.7^{+4.0}_{-0.6}$	$1.1^{+9.4}_{-1.1}$	2^{+15}_{-2}
z	Δt_{KN}	$0.8^{+2.3}_{-0.8}$	$1.6^{+1.6}_{-1.1}$	$2.0^{+2.3}_{-1.4}$	$1.8^{+3.0}_{-1.3}$	$1.8^{+2.7}_{-1.3}$	$1.8^{+2.6}_{-1.3}$	$1.6^{+2.9}_{-1.1}$	$1.6^{+3.1}_{-1.2}$	$1.7^{+2.8}_{-1.3}$
	Δt_{AG}	$0.14^{+0.69}_{-0.13}$	$0.16^{+0.89}_{-0.14}$	$0.2^{+1.2}_{-0.2}$	$0.3^{+1.7}_{-0.2}$	$0.4^{+2.6}_{-0.3}$	$0.5^{+4.0}_{-0.4}$	$0.7^{+6.3}_{-0.7}$	1^{+10}_{-1}	2^{+15}_{-2}
y	Δt_{KN}	$1.0^{+2.2}_{-1.0}$	$1.8^{+1.5}_{-1.7}$	$2.1^{+2.2}_{-1.7}$	$1.8^{+3.6}_{-1.4}$	$1.9^{+2.9}_{-1.4}$	$1.9^{+2.7}_{-1.4}$	$1.9^{+2.9}_{-1.4}$	$1.9^{+2.8}_{-1.5}$	$1.7^{+3.2}_{-1.4}$
	Δt_{AG}	$0.14^{+0.71}_{-0.12}$	$0.17^{+0.90}_{-0.15}$	$0.2^{+1.2}_{-0.2}$	$0.3^{+1.8}_{-0.2}$	$0.4^{+2.6}_{-0.3}$	$0.5^{+4.1}_{-0.5}$	$0.8^{+6.5}_{-0.7}$	1^{+10}_{-1}	2^{+16}_{-2}

NOTE—The values are the timescales during which the brightness of associated kilonova (Δt_{KN}) and afterglow (Δt_{AG}) is above the 5σ limiting magnitude in different bands with 90% interval.

we find that an one-day cadence strategy can always discover the highest number of kilonovae. For the choice of exposure time, kilonova detection rates by ZTF, WFST, and LSST would decline as the exposure time increases. On the contrary, a longer exposure time can discover more kilonova events for Mephisto, although the increase in the amount of discovered kilonovae with longer exposure times is not significant. Simultaneous imaging in three bands by Mephisto is the reason for the difference of the detection rates between Mephisto and other survey projects. To sum up, an one-day cadence strategy with a ~ 30 s exposure time is recommended to achieve optimal search for kilonovae. Based on Figure 2, the maximum kilonova detection rates for ZTF, Mephisto, WFST, and LSST are $\sim 0.3 \text{ yr}^{-1}$, $\sim 0.6 \text{ yr}^{-1}$, $\sim 1 \text{ yr}^{-1}$, and 20 yr^{-1} , respectively.

For afterglow-dominated events, there is no significant difference between searching in the optical and in the infrared bands for each survey project. The detection rates would drop with the increase of the exposure time. By adopting the optimal search strategy for kilonovae, one can also discover many afterglows from BNS mergers whose detection rate is much higher than that of kilonovae. For this case, the afterglow detection rates for ZTF, Mephisto, WFST, and LSST are $\sim 50 \text{ yr}^{-1}$, $\sim 60 \text{ yr}^{-1}$, $\sim 100 \text{ yr}^{-1}$, and $\sim 800 \text{ yr}^{-1}$, respectively.

3.4. Optimal Search Strategy for SiTian

SiTian (Liu et al. 2021; Yang et al. 2022a) is composed of a number of “units” deployed partly in China and partly at various sites around the world. Each unit includes three 1-m-class Schmidt telescopes with a FoV of $\Omega_{\text{FoV}} = 25 \text{ deg}^2$, which will simultaneously observe the same visit in three different optical filters. There will be also three or four 4-m-class telescopes for spectral identification and follow-up studies within the project.

SiTian at full design will scan at least $10,000 \text{ deg}^2$ of sky every 30 min, down to a detection limit of $g \approx 21 \text{ mag}$ with an exposure time of $\sim 1 \text{ min}$ using at least 14 units in China. Furthermore, at least 10 units outside China can survey an additional $\sim 20,000 \text{ deg}^2$ with a slightly lower cadence (a few hr). Based on this fiducial search plan of SiTian, we change the cadence time and exposure time for all of units to explore the optical search strategy of SiTian, while preserving the same sky coverage.

The results of the EM detection rates for SiTian are shown in Table 4. We show that SiTian can detect $\sim 2 \times 10^3 \text{ yr}^{-1}$ afterglow-dominated events. The detection rate of kilonova-dominated events is $\sim (2 - 4) \text{ yr}^{-1}$ by adopting the fiducial search plan of SiTian. Since kilonovae are very faint, a better search strategy would be to increase the exposure time of the telescopes with the expense of losing the cadence. The detection rate

Table 4. EM Detection Rates for SiTian

t_{exp}/s	$\Omega_{\text{FoV},1}/\text{deg}^2$	$t_{\text{cad},1}/\text{min}$	$\Omega_{\text{FoV},2}/\text{deg}^2$	$t_{\text{cad},2}/\text{min}$	$\dot{N}_{\text{KN}}/\text{yr}^{-1}$			$\dot{N}_{\text{AG}} \times 10^3/\text{yr}^{-1}$		
					g	r	i	g	r	i
45 (fiducial)		30		80	2.0	3.4	3.6	1.5	1.7	1.9
75	350	45	250	120	2.4	4.3	4.7	1.7	1.9	2.0
105		60		160	2.7	5.0	5.6	1.7	1.9	2.1
165		90		240	3.0	5.8	7.1	1.7	1.9	2.0

NOTE—We assume that the time between two visits is $t_{\text{oth}} = 15$ s. The operation times for units in China and outside China are assumed to be $t_{\text{ope}} = 8$ hr day $^{-1}$ and 16 hr day $^{-1}$, respectively. The columns are [1] the exposure time; [2] the total field of view of SiTian units in China; [3] the corresponding cadence time for SiTian units in China; [4] the total field of view of SiTian units outside China; [5] the corresponding cadence time for SiTian units outside China; [6-8] the detection rate of kilonova-dominated events in gri bands; [9-11] the detection rate of afterglow-dominated events in gri bands.

of kilonova-dominated events would slightly rise to $\sim (3 - 7)$ yr $^{-1}$ if an exposure time of 165 s is used.

3.5. Population Properties of Detectable EM Events via the Serendipitous Observations

By adopting an optimal serendipitous search strategy, i.e., an one-day cadence strategy, we show the redshift distributions of the detectable EM signals for a g -band limiting magnitude of $m_{g,\text{limit}} = 20, 22, 24,$ and 26 mag in Figure 4. As for each detectable EM signal, we randomly simulate the detection epochs a thousand times and calculate the median difference value between these detection epochs as the fading rate. Figure 5 shows the distributions of the fading rate for detectable EM signals. For the same search depth of each filter, there is no significant difference between searching in different bands. It is important to note that we collect all EM events whose $t_{\text{cad}} \geq 1$ day when we calculate the redshift distributions of the detectable EM signals, so that the distributions shown in Figure 4 do not consider their detection probabilities.

For a limiting magnitude of $m_{\text{limit}} = 20$ mag, the most likely EM counterpart of BNS mergers to be detected is individual sGRB emission. Due to this relatively shallow search depth, afterglow emissions associated with these individual sGRBs could have only at most one recorded epoch. In this case, it may be hard to establish the link between the sGRBs and the associated afterglows by the optically serendipitous searches. Detectable afterglow emissions should be much more easier to be discovered than kilonova emissions. However, these optical afterglows should be always associated with sGRB emissions. The most probable detectable redshift for these individual sGRBs and GRB-associated afterglows is $z \sim 0.5$, which is consistent with the observations (e.g., Fong et al. 2015). Some detectable orphan afterglows with much lower detection rate would take place at a range of $z \gtrsim 0.75$. In our simulations, the largest distance of the

detectable kilonovae is $z_{\text{max}} \sim 0.02$ ($D_{\text{L,max}} \sim 80$ Mpc). Most of ($\sim 80\% - 90\%$) these detectable kilonovae are expected to be discovered individually without the detections of accompanied sGRB emissions.

The improvement of the search depth would lead to a proportionate decrease in the individual detectable sGRB events. If $m_{\text{limit}} \gtrsim 22$ mag, more near-on-axis orphan afterglows and nearby off-axis orphan afterglows can be discovered, which would become the primary detectable EM counterparts of BNS mergers. For a limiting magnitude of $m_{\text{limit}} \gtrsim 24$ mag, one can always find the associated afterglow and kilonova emissions after the sGRB triggers via the optically serendipitous searches. Due to the limited instrument sensitivity of γ -ray telescopes, the largest distance of the sGRB-associated afterglows and kilonovae is $z_{\text{max}} \sim 1.75$. We note that this simulated largest distance of sGRB triggers is obtained by adopting an effective sensitivity limit of Fermi-GBM and GECAM. A few Swift sGRBs were found to have photometric redshifts of $z \gtrsim 2$ presented by Nugent et al. (2022), because Swift-BAT has a lower sensitivity compared with Fermi-GBM and GECAM, and hence a deeper detection depth. With the increase of the search depth, kilonovae would play a leading role of nearby detectable EM counterparts. For a limiting magnitude of $m_{g,\text{limit}} = 22, 24,$ and 26 mag, the median (largest) distances of these detectable kilonovae are $z = 0.04, 0.1,$ and 0.25 ($z_{\text{max}} = 0.06, 0.21,$ and 0.55). Search depth has little effect on the ratio between detectable kilonovae w/ sGRBs and kilonovae w/o sGRBs.

The fading rates of the detectable afterglows always peak at ~ 1.3 mag day $^{-1}$, which have a wide distribution between ~ -0.5 day $^{-1}$ and ~ 4.5 mag day $^{-1}$. Comparing with afterglows, kilonova-dominated events have more slow-evolving lightcurves. Their fading rates peak at $\sim 0 - 0.1$ mag day $^{-1}$. For a limiting magnitude of $m_{\text{limit}} \lesssim 22$ mag, the fading rates of kilonovae locate in a range from -0.25 day $^{-1}$ to ~ 1 mag day $^{-1}$.

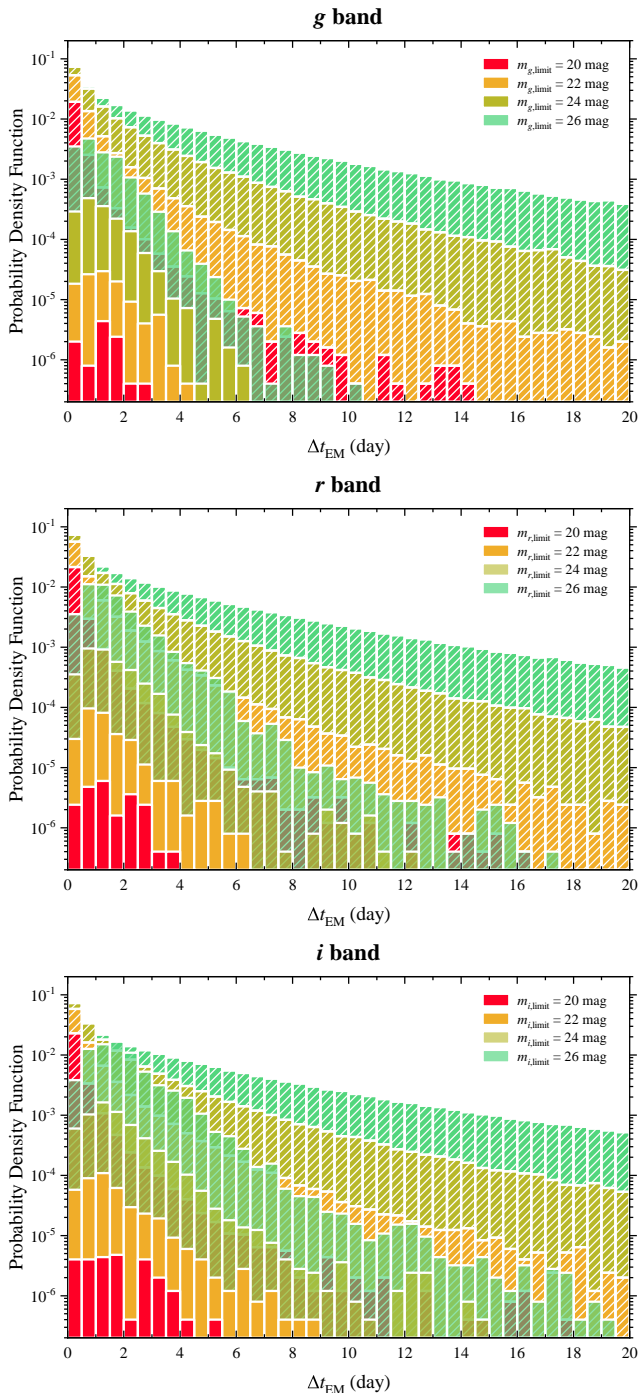


Figure 1. Crimson, orange, yellowgreen, and green histograms are the probability density functions of Δt_{KN} (solid histograms) and Δt_{AG} (striped histograms) for a limiting magnitude of $m_{\text{limit}} = 20, 22, 24,$ and 26 mag, in g band (top panel), r band (medium panel), and i band (bottom panel). The bin width of the histograms is set as $\Delta = 0.5$ day.

As shown in Figure 5, by adopting a limiting magnitude of $m_{\text{limit}} \gtrsim 24$ mag ($m_{\text{limit}} \gtrsim 26$ mag), some fast-evolving sGRB-associated kilonovae (kilonovae w/ sGRBs and kilonovae w/o sGRBs) with a fading rate of $\gtrsim 1$ mag day $^{-1}$ can be discovered. For these fast-evolving kilonova events, their early-stage observations would be contributed by the associated afterglows while the kilonova emissions would lead to the late-stage observations.

4. DETECTABILITY FOR TARGET-OF-OPPORTUNITY OBSERVATIONS OF GW TRIGGERS

4.1. GW Detectability Method

It is expected that two Advanced LIGO detectors (H1 and L1) in the USA (Harry & LIGO Scientific Collaboration 2010; LIGO Scientific Collaboration et al. 2015), Advanced Virgo detector (V1) in Europe (Acernese et al. 2015), and KAGRA detector (K1) in Japan (Aso et al. 2013; Kagra Collaboration et al. 2019) will start the fourth observation run (O4) together in 2023. The network composed of these 2nd generation detectors is referred to as the “HLV era” in the following. Here, the sensitivities of H1, L1 and V1 in the HLV era are adopted as their respective design sensitivities (Abbott et al. 2020a) since their sensitivities are dynamic and change over time⁵, while K1 is ignored in our simulations in view of that K1 will work to improve most of time in O4⁶. The 2nd generation detectors would finish their upgrade to 2.5th generation detectors in ~ 2025 . The subsequent upgrade of Advanced LIGO, Advanced Virgo, and KAGRA are called Advanced LIGO Plus (A+; Miller et al. 2015), Advanced Virgo Plus (AdV+; Abbott et al. 2020a), and KAGRA+ (Michimura et al. 2020). Hereafter, we refer to the era during which these four detectors upgrade to 2.5th generation detectors as the “PlusNetwork era”. After ~ 2030 , the 3rd generation GW detectors are expected to start their observation. The currently proposed 3rd generation detector plans include LIGO Voyager (Adhikari et al. 2020) as a possible upgrade upon LIGO A+ (strictly speaking, it’s more like quasi-3rd generation. However, since its sensitivity is much higher than that of the 2.5th generation detectors, for the convenience of discussion, we classify it as 3G), ET in Europe (Punturo et al. 2010a,b; Maggiore et al. 2020), and CE in the USA (Reitze et al.

⁵ We show differences between design sensitivity curves we use and latest sensitivity curves released on April 6th, 2022 in Figure 13 of Appendix A. Based on these latest sensitivity curves, our simulations of GW detection rate in O4 might be slightly overestimated.

⁶ <https://www.ligo.caltech.edu/news/ligo20220617>

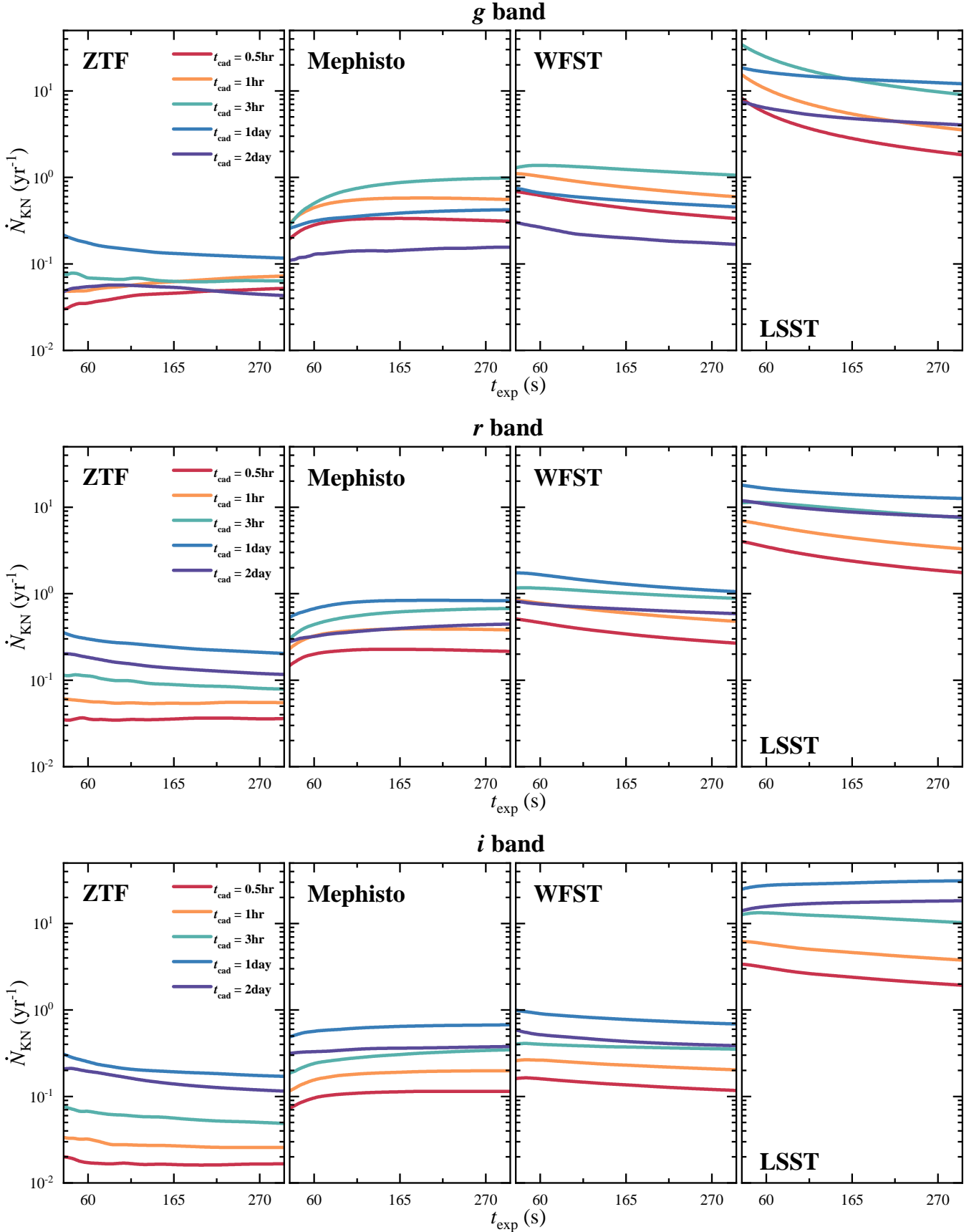


Figure 2. Detection rates of kilonova-dominated sample as functions of exposure time t_{exp} and cadence time t_{cad} for serendipitous observations. Four survey projects, including ZTF, Mephisto, WFST, and LSST (from left to right panels), are considered. The panels from top to bottom represent events of kilonova-dominated sample to be detected in the g band, r band, and i band, respectively. Red, orange, green, blue, and violet lines are the detection rates by adopting cadence searching strategies of $t_{\text{cad}} = 0.5$ hr, 1 hr, 3 hr, 1 day, and 2 day, respectively.

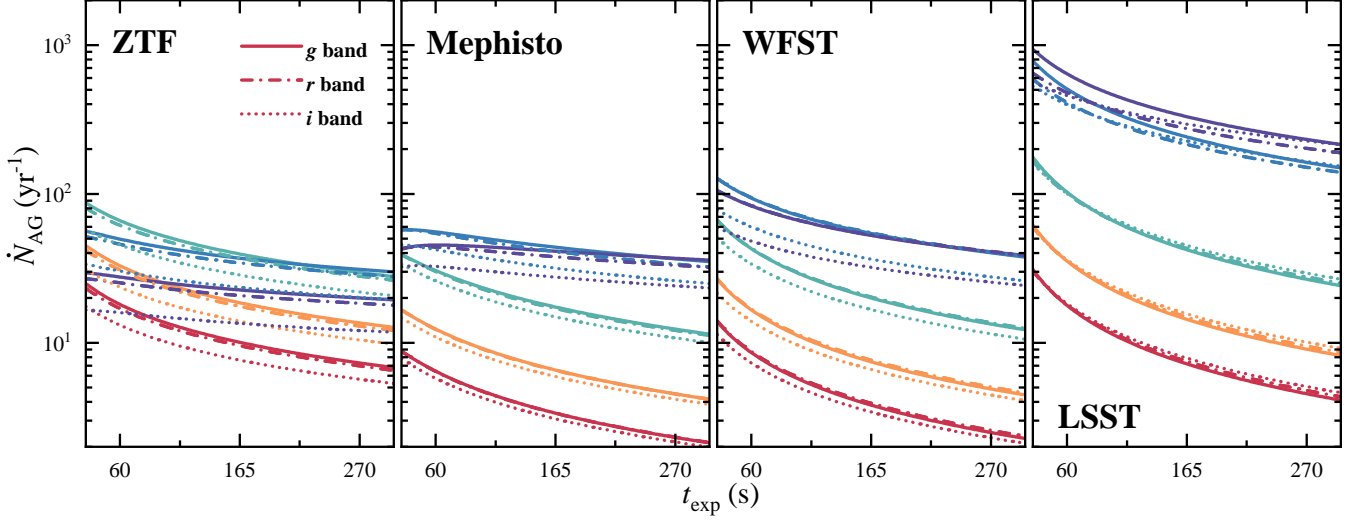


Figure 3. Similar to Figure 2, but for the detection rates of afterglow-dominated sample. Solid, dashed-dotted, and dotted lines represent the detection rates in g , r , and i band, respectively.

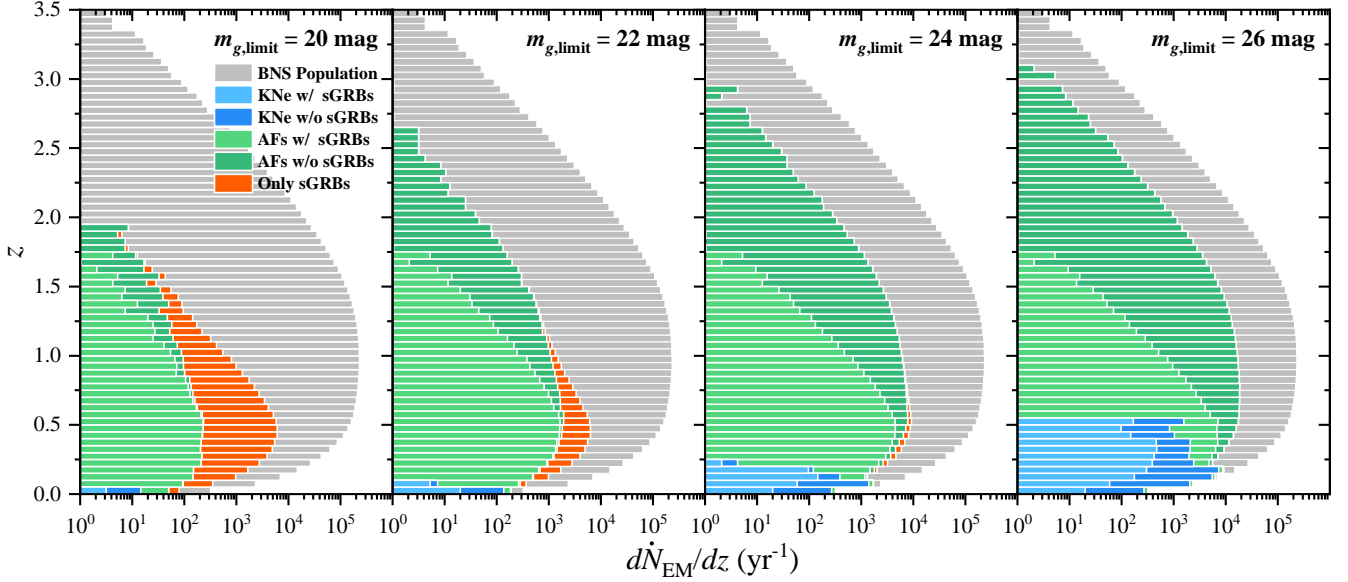


Figure 4. Redshift distributions of the detectable EM signals via the serendipitous searches for a g -band limiting magnitude of $m_{g,\text{limit}} = 20, 22, 24,$ and 26 mag (from left to right panels). Gray histograms are the redshift distributions of the simulated cosmological BNS population. The light blue, dark blue, light green, dark green, and orange histograms represent the redshift distributions for the detectable samples of kilonovae w/ sGRBs, kilonovae w/o sGRBs, afterglows w/ sGRBs, afterglows w/o sGRBs, and sGRBs only, respectively. The bin width of the histograms is set as $\Delta = 0.05$.

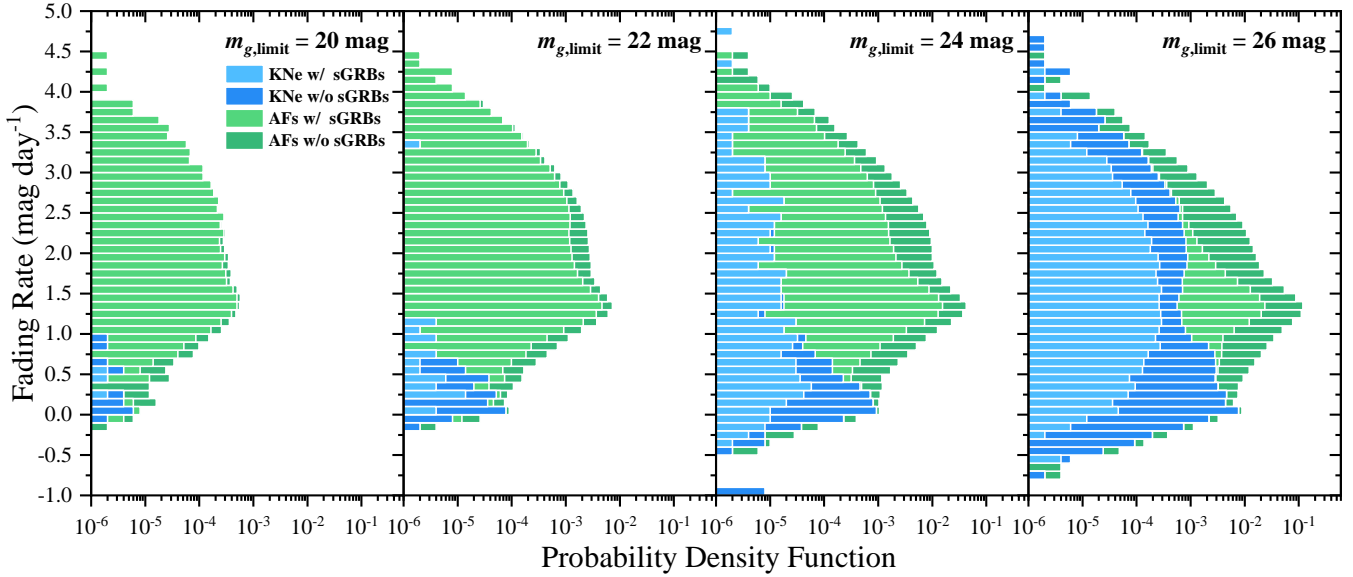


Figure 5. Similar to Figure 4, but for the g -band fading rates of the detectable EM signals. The bin width of the histograms is set as $\Delta = 0.1 \text{ mag day}^{-1}$.

2019). Due to the as-yet undetermined locations of ET and CE, we directly place ET at the current Virgo detector position and two CE detectors at the current H1 and L1 positions, according to the convention (Vitale & Evans 2017; Vitale & Whittle 2018).

For each BNS system, we randomly simulate the masses of individual NSs based on the observationally derived mass distribution of Galactic BNS systems, i.e., a normal distribution $M_{\text{NS}}/M_{\odot} \sim \mathcal{N}(1.32, 0.11^2)$ (Lattimer 2012; Kiziltan et al. 2013). The NS equation of state (EoS) DD2 (Typel et al. 2010), which is one of the stiffest EoS allowed by present constraints (e.g., Gao et al. 2016; Abbott et al. 2019), is adopted. With known M_{NS} , z , and EoS, we use the IMRPhenomPv2_NRTidalv2 (Dietrich et al. 2019) waveform model to simulate the GW waveform in the geocentric coordinate system, and then project it to different detectors to obtain the detector-frame strain signal. The optimal signal-to-noise ratio (S/N) can be obtained by

$$\rho_{\text{opt}}^2 = 4 \int_{f_{\text{min}}}^{f_{\text{max}}} \frac{|\tilde{h}(f)|^2}{S_n(f)} df = \int_{f_{\text{min}}}^{f_{\text{max}}} \frac{(2|\tilde{h}(f)|\sqrt{f})^2}{S_n(f)} d\ln(f), \quad (5)$$

where f is the frequency, $\tilde{h}(f)$ is the strain signal in the frequency domain, and $S_n(f)$ is the one-sided power spectral density of the GW detector which is square of the amplitude spectral density (ASD). The ASD for each detector is shown in the Appendix A. We set the maximum frequency f_{max} as 2048 Hz. The low frequency cutoff f_{min} is set to 20 Hz for O3, 10 Hz for all the 2nd, 2.5th generation detectors (Miller et al. 2015) and LIGO Voyager (Adhikari et al. 2020), 5 Hz for CE (Reitze et al.

Table 5. O3 duty cycle

Online Detector	P_{duty}
HLV	46.75%
HL	14.80%
HV	9.68%
LV	11.8%
H	3.06%
L	2.94%
V	7.59%
None	3.35%

2019), and 1 Hz for ET (Punturo et al. 2010a). We use the optimal S/N to approximate the matched filtering S/N of the GW signal detected by each detector, and then calculate the network S/N of the entire detector network, i.e., the root sum squared of the S/N of all detectors. In each GW era, when the S/N for a single detector is greater than the threshold of 8 and the network S/N is greater than 12, we expect that the corresponding GW signal is detected.

We consider the exact duty cycle of O3 (see Table 5), calculated following the timeline released from LVC⁷, to simulate the GW observations of BNS mergers in O3 and O4. In view of significant technology upgrades for GW detections and more detectors that will join GW campaigns, the duty cycle in the 2.5th and 3rd generation detector networks could be highly uncertain. Thus, we only calculate their best cases, i.e., “all detectors in

⁷ <https://www.gw-openscience.org/O3/index/>

the corresponding era have reached the design sensitivity and work normally” as the optimal situation. During the 2.5th generation detector network, the best case is that A+, Adv+, and KAGRA+ all work normally, which we abbreviate as “PlusNetwork”. LIGO Voyager is separately discussed. Furthermore, “ET&CE” represents the best case of the 3rd generation era.

We need to localize the BNS through GW signals for EM follow-ups. Since we need to calculate a large number of simulated signals, we use Fisher Information Matrix (FIM; Cutler & Flanagan 1994) to approximate the localization area estimated by the more computationally expensive Bayesian method (Thrane & Talbot 2019). The FIM is based on the Linear Signal Approximation (LSA; Cutler & Flanagan 1994), and uses a Gaussian distribution to approximate the posterior distribution of the parameters. This assumption requires the signal to have a sufficiently high S/N, so we only calculate the GW localization for the signal whose network S/N meets the detection threshold. The FIM of the detector network is a linear summation of the FIM of the individual detector in that network

$$\mathbf{\Gamma}_{ij} = \sum_k \langle \partial_i h | \partial_j h \rangle_k, \quad (6)$$

where the bracket means the inner product

$$\langle a | b \rangle = 4\Re \int_{f_{\min}}^{f_{\max}} \frac{\tilde{a}(f)\tilde{b}^*(f)}{S_n(f)} df, \quad (7)$$

k is the index of the detector in that network, $\partial_i h$ or $\partial_j h$ refers to the partial differentiation of the detector-frame signal in the frequency domain with respect to a certain parameter. In our FIM calculation, the parameters are chosen from the detector-frame chirp mass \mathcal{M} , the symmetric mass ratio η , the luminosity distance D_L , the coalescence time t_c , the coalescence phase ϕ_c , the inclination angle l , the polarization angle ψ , the right ascension θ , the declination ϕ , and the tidal deformation parameters $\tilde{\Lambda}$ and $\delta\tilde{\Lambda}$. Note that, for the 3rd generation detector network, we also take the Earth’s rotation into account (Liu & Shao 2022). In order to reduce the matrix singularity issue, we don’t take partial differentiation of the tidal parameters for the cases before the 3rd generation.

For high-S/N signals, the inverse of the FIM is less or equal to the covariance matrix of parameters, the so-called “Cramer-Rao lower bound”

$$\text{cov}(i, j) \geq (\mathbf{\Gamma}^{-1})_{ij}, \quad (8)$$

for a specific parameter, we can use the square root of the corresponding diagonal element in the inverse of the

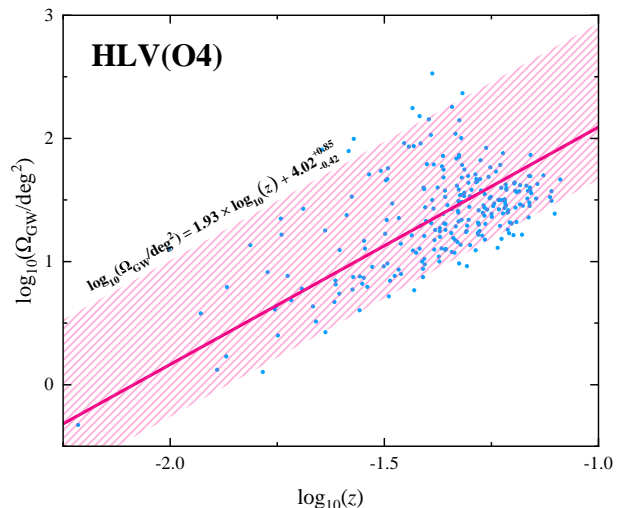


Figure 6. 90% confidence of GW sky localization vs. redshift for BNS mergers detected at the HLV (O4) era when all three GW detectors are online at the same time.

FIM as the bias. In our case, we care about $\Delta \cos \theta$ and $\Delta \phi$. Then we can get the sky localization area (Barack & Cutler 2004)

$$\Omega_{\text{GW}} = 2\pi \sqrt{(\Delta \cos \theta \Delta \phi)^2 - \langle \Delta \cos \theta \Delta \phi \rangle^2}, \quad (9)$$

we use 90% confidence of this area hereafter.

4.2. GW Detections and EM Follow-ups in the 2nd Generation Era

4.2.1. GW Detection Rate, Detectable Distance, and Sky Localization

By considering an exact duty cycle shown in Table 5, the simulated GW detection results of O3 and O4 are summarized in Table 6. We check that the GW detection rate in O3 should be $\sim 2.4_{-1.8}^{+3.6} \text{ yr}^{-1}$, which is consistent with the observations of LVC (Abbott et al. 2020a, 2021c). The median detectable luminosity distance is ~ 110 Mpc, nearly approximate to the observed distance of GW190425 (Abbott et al. 2020b). In the HLV (O4) era, we predict that one can detect $\sim 11 \text{ yr}^{-1}$ BNS GW events with a median detectable distance at $z \sim 0.040$ and a horizon at $z_{\max} \sim 0.084$.

We simulate the sky localization area (Ω_{GW}) for detectable BNS GW events when two or three detectors are online simultaneously during O4. Since the localization for GW mainly rely on the time delay between different detectors, so one 2nd generation GW detector is impossible to localize GW signals. We find that the relationship between the sky localization and redshift for BNS mergers detected in O4 with the H1, L1 and VIRGO network can be well explained by a log-linear trend (Figure 6), while the log-linear relationships with only two

Table 6. GW Detection Results

Case	Era	$\dot{N}_{\text{GW}}/\text{yr}^{-1}$ ($\dot{N}_{\text{GW}}/\dot{N}_{\text{BNS}}$)	z ($D_L/100$ Mpc)	z_{max} ($D_{L,\text{max}}/100$ Mpc)	$\log_{10}(\Omega_{\text{GW}}/\text{deg}^2) = a \times \log_{10}(z) + b$	
					a	b
HLV (O3)	2nd	$2.4^{+3.6}_{-1.8}$ (0.001%)	$0.025^{+0.025}_{-0.013}$ ($1.1^{+1.2}_{-0.5}$)	0.062 (2.9)	—	—
HLV (O4)	2nd	11^{+17}_{-8} (0.004%)	$0.040^{+0.025}_{-0.025}$ ($1.8^{+1.2}_{-1.1}$)	0.084 (4.0)	1.93	$4.02^{+0.85}_{-0.42}$
PlusNetwork	2.5th	210^{+320}_{-160} (0.08%)	$0.099^{+0.050}_{-0.055}$ ($4.7^{+2.6}_{-2.7}$)	0.190 (9.5)	1.87	$2.85^{+0.45}_{-0.55}$
LIGO Voyager	3rd	$1.8^{+2.8}_{-1.4} \times 10^3$ (0.73%)	$0.22^{+0.12}_{-0.13}$ ($11.0^{+7.4}_{-6.7}$)	0.43 (24.3)	—	—
ET&CE	3rd	$2.4^{+3.6}_{-1.8} \times 10^5$ (90.7%)	$0.97^{+0.71}_{-0.57}$ (65^{+64}_{-43})	3.77 (343)	2.00	$0.85^{+0.69}_{-0.46}$

NOTE—GW detection rates and luminosity distance distributions for detectable GWs in the 2nd generation era are simulated by adopting an exact duty cycle labeled in Table 5, while GW detection results in the 2.5th and 3rd generation eras are obtained with consideration of ideal operation conditions. The columns are [1] the case of different generation eras; [2] the generation of GW detectors; [3] median GW detection rates with consideration of 90% interval by adopting the local event rate density of $\dot{\rho}_{0,\text{BNS}} = 320^{+490}_{-240} \text{Gpc}^{-3} \text{yr}^{-1}$ (Abbott et al. 2021b), while the numbers in brackets are the corresponding detectable proportions of the number of BNS mergers per year in the universe (\dot{N}_{BNS}); [4] median detectable redshifts and detectable luminosity distances with consideration of 90% intervals; [5] maximum detectable redshifts and detectable luminosity distances; [6] GW sky localizations as function of z , where a and b are fitting parameters.

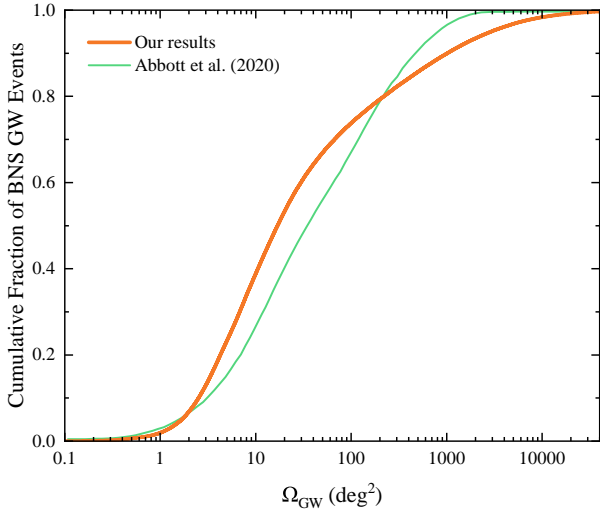


Figure 7. The cumulative fractions of BNS GW events with sky localization area during O4 smaller than the abscissa value. Our simulation results are marked as thick orange line, while model distribution from Abbott et al. (2020a) is shown as thin green.

GW detectors network are not obvious due to their limited detections. In Figure 7, the median sky localization area is expected to be $\sim 10 \text{deg}^2$ for detectable BNS GW events. We also collected the cumulative fraction of the sky localization from Abbott et al. (2020a). Comparing with our simulation, they considered the operation of K1 in O4 and used BAYESTAR (Singer & Price 2016) code to perform sky localization of BNS GW events. A

duty cycle of 70% for each detector uncorrelated with the other detectors, which is slightly different with our simulations, was adopted by Abbott et al. (2020a). However, our simulation result for the sky localization in O4 is nearly consistent with that shown in Abbott et al. (2020a).

4.2.2. EM Detectability in O4

Based on the BNS GW detection results during O4, we now estimate the EM detection rates of detectable BNS GW events for ZTF, SiTian, Mephisto, WFST, and LSST. For the serendipitous observations, the event would appear in an arbitrary position of the celestial sphere due to the lack of the ToO alerts. For the GW-triggered ToO observations, the survey project would just need to cover the sky localization of GW events in search of their associated EM counterparts. Thus, one can replace Ω_{sph} with Ω_{GW} in Equation (4) to estimate the EM detection rate for the ToO observations, i.e.,

$$\begin{aligned} \dot{N}_{\text{EM}} \approx & \frac{\dot{N}_{\text{BNS}}}{n_{\text{sim}}} \cdot \frac{\Omega_{\text{cov}}}{\Omega_{\text{sph}}} \\ & \times \sum_{i=1}^{n_{\text{GW}}} \sum_j \frac{\Omega_{\text{FoV}} P_{\text{duty},j} \min(t_{\text{cad},ij}, \Delta t_{ij})}{\max(\Omega_{\text{FoV}}, \Omega_{\text{GW},j}) (n_{\text{exp},ij} t_{\text{exp},ij} + t_{\text{oth}})}, \end{aligned} \quad (10)$$

where $j = \{\text{HL}, \text{HV}, \text{LV}, \text{HLV}\}$ and n_{GW} represents detectable BNS GW events. Here, we adopt $t_{\text{exp}} = 300 \text{s}$ to make GW-triggered follow-up observations. Thus, the

cadence time t_{cad} for each event is related to t_{exp} and Ω_{GW} for each event. The judgement condition for the detection of the kilonova and/or afterglow by a follow-up search after GW triggers is required to be *two different exposure filters have at least two detection epochs*.

Since SiTian will not operate during O4, we only show our simulated detection rates for ZTF, Mephisto, WFST and LSST at this era. Based on the technical informations of the survey projects listed in Table 2, our simulation results show that ZTF/SiTian/Mephisto/WFST/LSST can detect $\sim 5/4/3/3$ kilonovae ($\sim 1/1/1/1$ afterglows) in O4, respectively. $\sim 5\%$ kilonovae and $\sim 90\%$ afterglows after GW triggers are expected to be associated with the detections of sGRBs.

4.3. GW Detections and EM Follow-ups in the 2.5th and 3rd Generation Eras

4.3.1. GW Detection Rate, Detectable Distance, and Sky Localization

We summarize all our simulated GW detection results of 2.5th and 3rd generation eras in Table 6. The total mass, S/N, and redshift for detectable GW signals in different eras are shown in Figure 8. For the 2.5th generation GW detector network, the optimal detection rate is $\sim 210 \text{ yr}^{-1}$. The GW detection distance would be doubled compared with the detection distance in O4, i.e., the horizon can reach $z_{\text{max}} \sim 0.2$. For the LIGO Voyager in the 3rd generation era, the optimal detection rate can be increased to $\sim 1,800 \text{ yr}^{-1}$ and the detection distance would be twice compared with the last era, i.e., a horizon of $z_{\text{max}} \sim 0.4$. However, these numbers are much smaller than those for the newly designed 3rd generation detectors. For the ET&CE network, the optimal detection rate would be $\sim 2.4 \times 10^5 \text{ yr}^{-1}$ which would account for $\sim 91\%$ of the total BNS GW events in the universe. The events detected by ET&CE are mainly dominated by BNS mergers at $z \sim 1$, which is near the most probable redshift where BNS mergers occurred in the universe. The most remote detectable events by ET&CE would be at $z_{\text{max}} \sim 3.8$. Except for the ET&CE era, the median distance of detectable GW events is always set at half of the horizon in each GW era.

In Figure 9, the relationships between the 90% credible area of GW sky localization and redshift for BNS mergers detected at the PlusNetwork, LIGO Voyager and ET&CE eras can be represented by log-linear trends, similar to that of 2nd generation network. The fitting results of these log-linear trends are listed in Table 6. In the PlusNetwork era, most of detectable BNS mergers will be localized to $\lesssim 10 \text{ deg}^2$. The network of one ET detector and two CE detectors can have a

more remarkable capability to observe and localize BNS GW events. For BNS mergers that occurring at $z \lesssim 0.2$, the GW sky localizations constrained in the ET&CE era will be about two orders of magnitude lower than those constrained in the PlusNetwork era. The median localization for BNS mergers at $z \sim 0.5$ ($z \sim 1$) is shown to be $\sim 1 \text{ deg}^2$ ($\sim 10 \text{ deg}^2$). In these regimes, the present and future wide-field-of-view survey projects will be able to cover the sky localizations given by GW detections in a few pointings and achieve deep detection depths with relatively short exposure integration times. In view of that current GW operation plan during the LIGO Voyager era only includes two GW detectors, we find that the sky localizations will span from a few hundred square degrees to tens of thousands of square degrees. Thus, EM follow-ups might be very difficult if there are no more GW detectors join the campaign at the LIGO Voyager era.

4.3.2. EM Detectability

The BNS GW detectabilities for the networks of 2.5th, and 3rd generation GW detectors have been studied in detail in Section 4.3.1. Based on these results, we now discuss the EM detection probabilities and optimistic EM detection rates for GW-triggered ToO observations.

Since the luminosity distributions in different bands are consistent, we only show g -band luminosity distributions for the EM signals of detectable GW events at different GW eras in Figure 10. For the future GW eras of PlusNetwork, LIGO Voyager, and ET&CE, the critical magnitudes for the detection of EM emissions from all BNS GW events would be $\sim 23.5 \text{ mag}$, $\sim 25 \text{ mag}$, and $\gtrsim 26 \text{ mag}$, respectively. Present and foreseeable future survey projects can hardly find all EM signals of BNS GW events detected during the ET&CE era. Comparing with the results of adjacent GW eras, one can see there appears little difference in the number of detectable kilonovae if adopting a detection depth as the critical magnitude of earlier GW era. However, one can find much more remote sGRBs and afterglows in the later GW era. As the search limiting magnitude increases, the amount of detectable kilonovae would increase exponentially. There is also an exponential increase with a slower rising slope for the amount of afterglows. At the critical magnitude of each era, $\sim 80\%$ BNS GW events can observe clear kilonova signals, while afterglows would account for the other $\sim 20\%$ BNS GW events. Most of the detectable kilonova-dominated BNS GW events would be not accompanied with the observations of sGRBs. The kilonova events associated with sGRBs like the observations of GW170817/GRB170817A/AT2017gfo would be scarce.

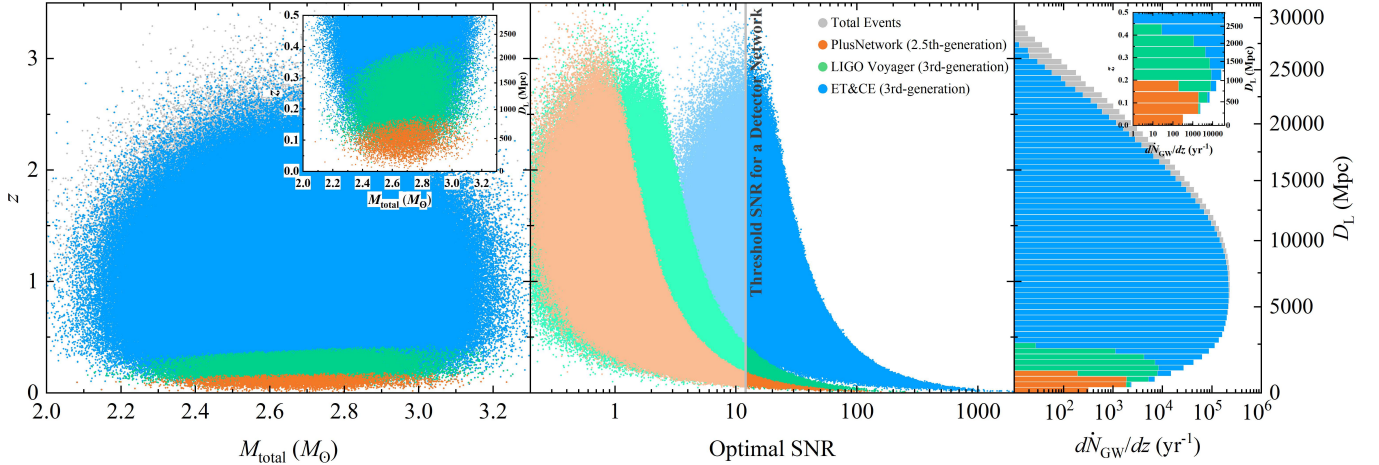


Figure 8. Detectability of BNS mergers by various detector networks in different GW detection eras. The left panels show the signals that can be detected by different detectors and detector networks. The orange, green, and blue dots are the GW signals detectable at PlusNetwork, LIGO Voyager, and ET&CE network eras, respectively. The gray dots in the background represent undetectable signals. The small panels in the upper right corner are enlarged images of the low-redshift area. The middle panels show the distributions of all simulated signals on the “optimal S/N–redshift” plane, with detection thresholds for a detector network (i.e., $S/N = 12$; light gray line). To the right of the thresholds are the GW signals that can be detected. The right panels show the distributions of BNS detection rates with redshift, and the insets are zoom-in pictures in the low-redshift region.

Based on the GW detections in different eras, we then estimate the optimistic EM detection rates for specific survey projects listed in Table 2. In ideal operation conditions of the PlusNetwork and ET&CE eras, due to precise sky localizations of GW events, these survey projects will be able to cover the sky localizations given by GW detections in a few pointings. Thus, we define $\Omega_{\text{cov}}/\Omega_{\text{GW}} \sim 1$ in Equation (10) to estimate the EM detection rates. We note that although the current plan at the LIGO Voyager era shows relatively poor sky localization for GW events, we still estimate the EM detection rate of this era by defining $\Omega_{\text{cov}}/\Omega_{\text{GW}} \sim 1$ under the assumption that more GW detectors will join the campaign might significantly improve the sky localizations. The optimistic detection rates of EM signals at different GW eras for specific survey projects are displayed in Figure 11 and labeled in Table 7. By comparing the limiting magnitudes of specific survey projects and the critical magnitudes in the different GW eras (Figure 10), we find that these wide-field surveys (ZTF, SiTian, Mephisto, and WFST) are unlikely to detect a larger number of kilonovae despite the upgraded GW detectors improving BNS detection rates. Optimistically, ZTF/SiTian/Mephisto/WFST can detect $\sim 5/5/150/120$ kilonovae per year at the 2.5th and 3rd generation era, while $\sim 100/300/1200 \text{ yr}^{-1}$ kilonovae per year can be discovered by LSST during the PlusNetwork/LIGO Voyager/ET&CE eras, respectively. At later GW era, ToO observations of BNS GW events can always discover more afterglows, almost all of which

are associated with sGRBs. However, we find a special case that LSST follow-up in the ET&CE era will detect as much as $\sim 75\%$ of detectable afterglows, which will largely orphans unaccompanied by an sGRB.

5. CONCLUSIONS AND DISCUSSION

In this paper, based on our model proposed in the companion paper (Paper I), we have presented the serendipitous search detectability of time-domain surveys for BNS EM signals, the detectability of GWs for different generations of GW detectors, as well as joint-search GW signals and optical EM counterparts⁸.

Serendipitous observations—We have systematically made simulations of optimal search strategy for searching for kilonova and afterglow emissions from BNS mergers by serendipitous observations. For our selected survey projects, which include ZTF/Mephisto/WFST/LSST, we have found that a one-day cadence serendipitous search with an exposure time of ~ 30 s can always achieve near maximum detection rates for kilonovae and afterglows. The optimal detection rate of kilonova-dominated (afterglow-dominated) events are $\sim 0.3/0.6/1/20 \text{ yr}^{-1}$ ($\sim 50/60/100/800 \text{ yr}^{-1}$), respectively, for the survey projects of ZTF/Mephisto/WFST/LSST. As for the survey array of SiTian project, we have shown that when

⁸ GW and EM detectability in the decihertz GW band could be found in Liu et al. (2022) and Kang et al. (2022).

Table 7. *g*-band optimistic EM Detection Rates in Each GW Era

Sample	Era	ZTF	SiTian	Mephisto	WFST	LSST
KNe w/ sGRBs	PlusNetwork	0.8	0.9	6.3	4.9	4.9
	Voyager	0.8	0.9	16.6	12.8	22.1
	ET&CE	0.8	0.9	23.6	18.1	75.4
KNe w/o sGRBs	PlusNetwork	4.0	4.4	82.4	63.4	74.0
	Voyager	4.0	4.4	118	90.9	438
	ET&CE	4.0	4.4	130	100	1.11×10^3
AFs w/ sGRBs	PlusNetwork	16.8	16.8	27.1	20.9	20.9
	Voyager	36.6	36.6	154	118	131
	ET&CE	101	101	905	696	1.37×10^3
AFs w/o sGRBs	PlusNetwork	0.4	0.5	3.1	2.4	2.4
	Voyager	0.7	0.7	36.2	27.9	47.4
	ET&CE	3.3	3.3	392	302	2.93×10^3
ToTal EM Signals	PlusNetwork	22.1	22.6	119	91.5	102
	Voyager	42.2	42.7	325	250	639
	ET&CE	109	110	1.45×10^3	1.12×10^3	5.49×10^3

NOTE—The values represent the simulated BNS merger detection rates (in unit of yr^{-1}) in different GW eras.

the array fully operates it will discover more kilonova events if a longer exposure time is adopted. The detection rate of kilonova (afterglow) events could even reach $\sim 7(2 \times 10^3)\text{yr}^{-1}$ by SiTian. The population properties and fading rates of the detectable kilonovae and afterglows have been studied in detail. Our results have shown that afterglows are easier to detect than kilonovae by these survey projects. These afterglows detected via the optically serendipitous observations should be always associated with sGRBs. However, present survey projects have not detected as many afterglows as we have predicted. One reason may be that only part of BNS GW events could generate relativistic jets and power bright afterglows (e.g., Sarin et al. 2022). Genuine weather fluctuations and operational issues of optical telescopes might contribute to the deficit of detection. Actual survey observations can hardly always achieve the prospective detection depth and cadence, which could be another cause of the lack of enough afterglow observations. Furthermore, the relatively longer cadence interval for traditional survey projects have been designed to discover ordinary supernovae or tidal disruption events. These cadence intervals are significantly larger than the timescales during which the brightness of afterglow is above the limiting magnitude (as shown in Table 3), so afterglow events could be easily missed. Recently, thanks to the improved cadence, ZTF has discovered seven independent optically-discovered GRB afterglows without any detec-

tion of an associated kilonova (Andreoni et al. 2021b). Among these detected afterglows, at least one event was inferred to be associated with a sGRB. This ZTF observation may support our afterglow simulations, but also show a possible low efficiency of detecting afterglows. Thus, such selection criteria may miss most of kilonova events. Conversely, the low efficiency of afterglow observations also indicate the difficulty for searching for kilonova signals by serendipitous observations. Andreoni et al. (2021a,b) intended to select kilonova and afterglow candidates from survey database by considering recorded sources having rising rates faster than 1 mag day^{-1} and fading rates faster than 0.3 mag day^{-1} . When $m_{\text{limit}} \lesssim 22 \text{ mag}$, our detailed studies on the population properties of detectable kilonovae and afterglows reveal that their detected fading rates peak at $\sim 0 - 0.1 \text{ mag day}^{-1}$ and $\sim 1.3 \text{ mag day}^{-1}$, respectively.

GW detections and ToO follow-ups during O4—By applying the duty cycle of O3 to simulate the GW observations during O4, we predict that one can detect $\sim 11 \text{ yr}^{-1}$ BNS GW events with a median detectable distance at $z \sim 0.040$ and a horizon at $z_{\text{max}} \sim 0.084$. The median sky localization area is expected to be $\sim 10 \text{ deg}^2$ for detectable BNS GW events in O4. Based on the public alert distributions in O3, Petrov et al. (2022) suggested that the threshold S/N for the detection of BNSs might be lower (i.e., $S/N > 9$). Following their suggestions, the detection rate of BNS mergers would be higher and the median GW sky localization area would

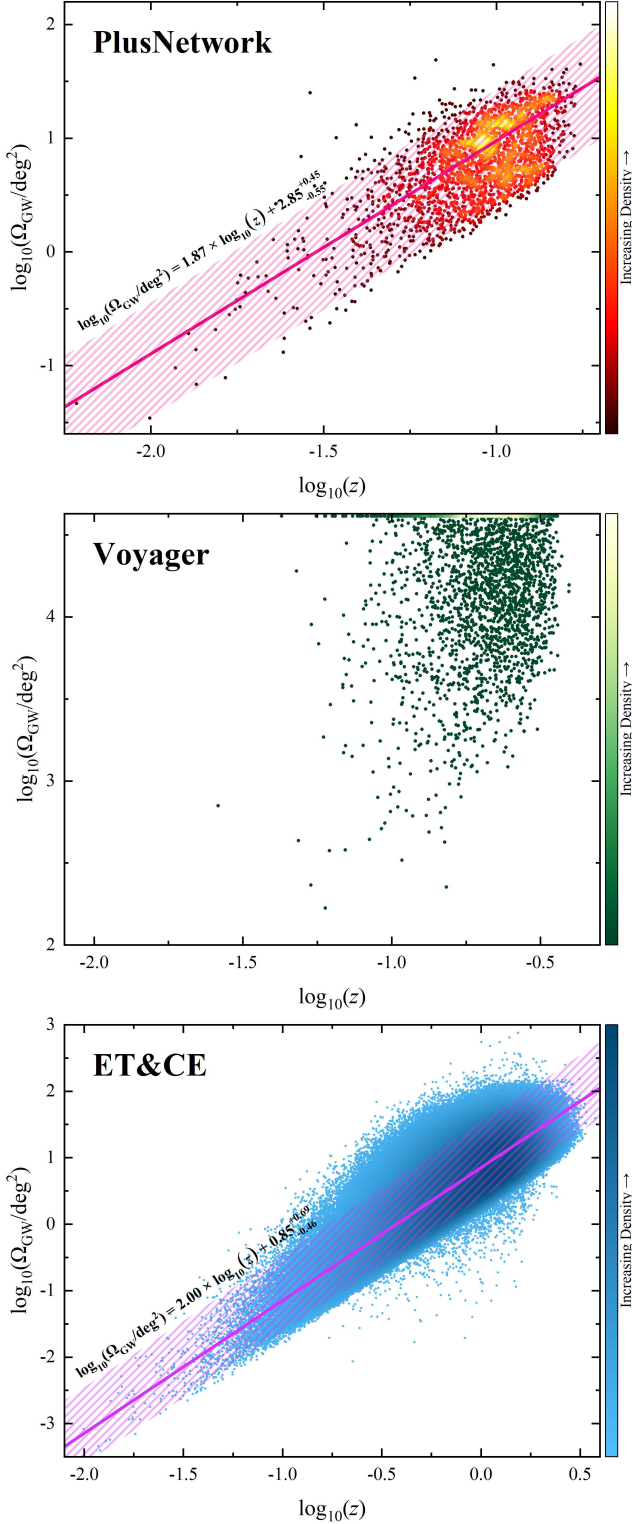


Figure 9. 90% confidence of GW sky localization vs. redshift for BNS mergers detected at the PlusNetwork (top panel), LIGO Voyager (middle panel) and ET&CE eras, respectively. The density (see the colorbar of each panel) for the points is calculated via the kernel density estimation. Solid line and shaded region in each panel represent the median of the GW sky localization and 90% interval, respectively.

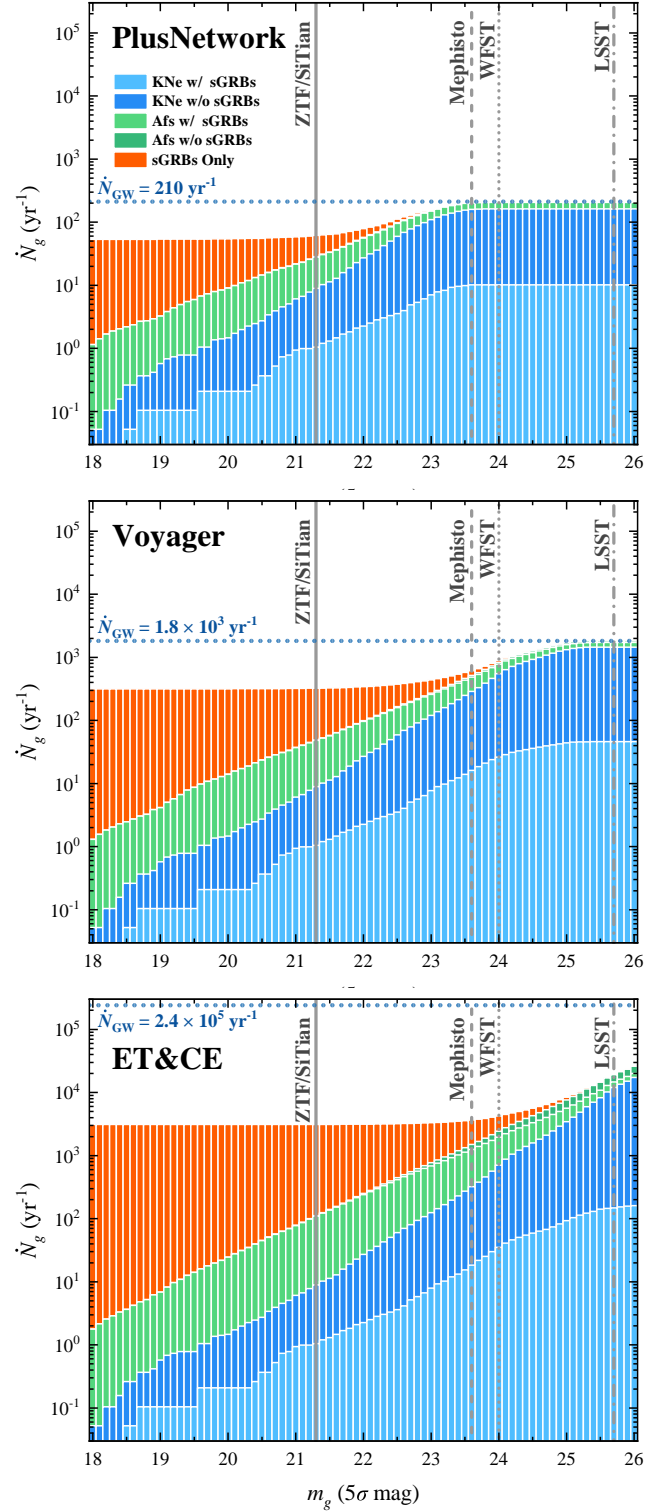


Figure 10. g -band luminosity functions for the detectable samples of kilonovae w/ sGRBs (light blue histograms), kilonovae w/o sGRBs, (dark blue histograms), afterglows w/ sGRBs (light green histograms), afterglow w/o sGRBs (dark green histograms), and only sGRBs (orange histograms) as functions of g -band 5σ limiting magnitude during three GW detection eras, i.e., the PlusNetwork, LIGO Voyager, and ET&CE eras. The gray solid, dashed, dotted, and dashed-dotted lines respectively represent the r -band 5σ limiting magnitude of ZTF/SiTian, Mephisto, WFST, and LSST, with 300 s exposure time. The dashed blue lines show the GW detection rates in each GW era. The bin width of the histograms is set as $\Delta = 0.1$ mag.

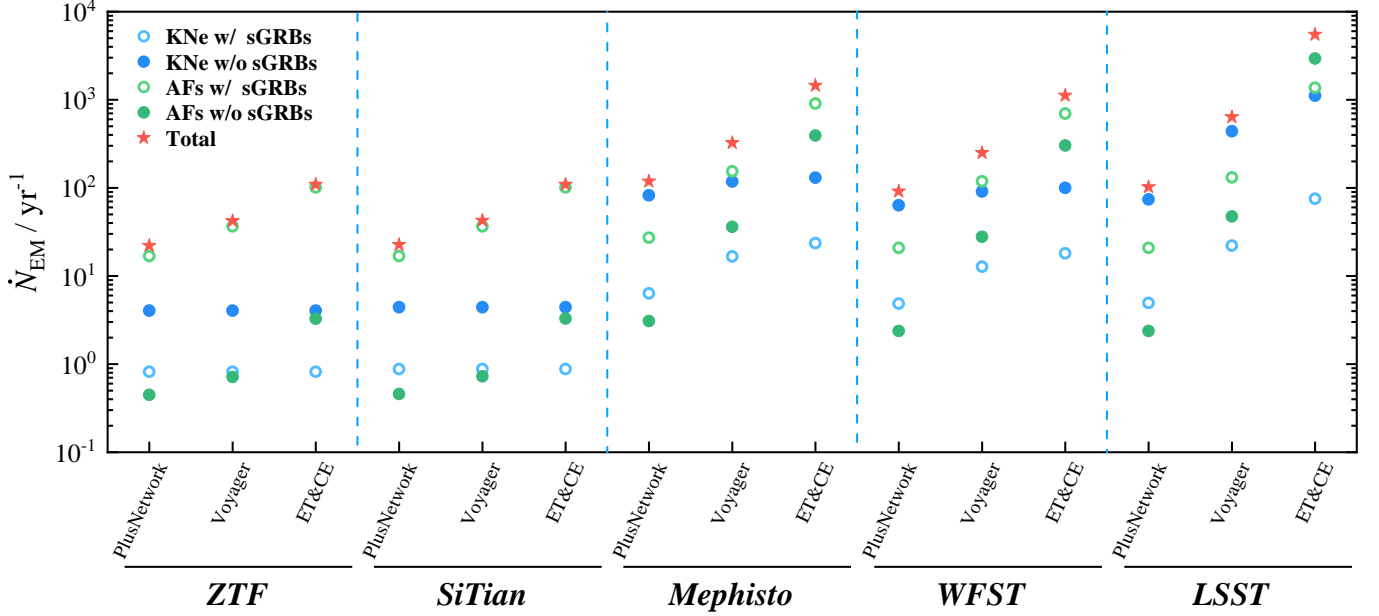


Figure 11. g -band optimistic detection rates of kilonovae w/ sGRBs (light blue circles), kilonovae w/o sGRBs (dark blue circles), afterglows w/ sGRBs (light green circles), afterglows w/o sGRBs (dark blue circles) and total EM signals (red stars) for specific survey projects (including ZTF, SiTian, Mephisto, WFST, and LSST) in the PlusNetwork, Voyager, and ET&CE eras.

be larger in O4 by comparison with our simulations. In this paper, we adopt their respective design sensitivities to simulate GW detections and ToO follow-ups of GW triggers since their sensitivities are dynamic and change over time. After the completion of this work, we notice that detection sensitivities of H1, L1, V1, and K1 in upcoming O4 have been updated⁹. Based on their latest detection sensitivities, our simulations for the detection rate, detectable distance, and sky localization might be slightly better than they will really be. During O4, our simulations show that ZTF/Mephisto/WFST/LSST will detect $\sim 5/4/3/3$ kilonovae ($\sim 1/1/1/1$ afterglows) per year, respectively. Most of these detectable afterglows are expected to be associated with sGRBs, while only $\lesssim 5\%$ kilonovae can simultaneously detect their associated sGRBs after GW triggers.

GW detections and ToO follow-ups at the 2.5th and 3rd generation eras — We have carried out detailed calculations of the detection capabilities of the 2.5th and 3rd generation detector networks in the near future for BNS GW signals. Optimistically, we show that the GW detection rate and detection horizon for the PlusNetwork are $\sim 210 \text{ yr}^{-1}$ and $z_{\text{max}} \sim 0.2$, respectively. Most of detectable BNS mergers will be localized to $\lesssim 10 \text{ deg}^2$, which are always smaller than the FoV of most of the survey projects. For the LIGO Voyager in the 3rd gener-

ation era, the optimal detection rate can be increased to $\sim 1,800 \text{ yr}^{-1}$ and the detection distance would be twice compared with the last era, i.e., a horizon of $z_{\text{max}} \sim 0.4$. The ET&CE network is expected to detect all BNS merger events in the entire universe, with detection rates $\sim 2.4 \times 10^5 \text{ yr}^{-1}$. As the sensitivity of GW detectors increases, BNS events at high redshifts gradually dominate the detected events. At this era, the detection rate is mainly dominated by BNS mergers at $z \sim 1$. The median localization for BNS mergers at $z \sim 0.5$ ($z \sim 1$) is shown to be $\sim 1 \text{ deg}^2$ ($\sim 10 \text{ deg}^2$). In the PlusNetwork and LIGO Voyager eras, the critical magnitudes for the detection of EM emissions from all BNS GW events would be $\sim 23.5 \text{ mag}$ and $\sim 25 \text{ mag}$, respectively. At the critical magnitude of each era, $\sim 80\%$ BNS GW events can observe clear kilonova signals, while afterglows would account for the other $\sim 20\%$ BNS GW events. ZTF/SiTian/Mephisto/WFST can optimistically detect $\sim 5/5/150/120$ kilonovae per year at the 2.5th and 3rd generation era, while $\sim 100/300/1200 \text{ yr}^{-1}$ kilonovae per year can be discovered by LSST during the PlusNetwork/LIGO Voyager/ET&CE eras, respectively. At later GW era, ToO observations of BNS GW events can always discover more afterglows, almost all of which are associated with sGRBs. Present and foreseeable future survey projects can hardly find all EM signals of BNS GW events detected during the ET&CE era. By assuming a single-Gaussian structured jet model (e.g., Zhang & Mészáros 2002), we have shown that

⁹ <https://observing.docs.ligo.org/plan/>.

GW170817-like events, which can be simultaneously observed as an off-axis sGRB and a clear kilonova, may be scarce. In order to explain the sGRB signal of GW170817/GRB170817A, a two-Gaussian structured jet model may be required (Tan & Yu 2020). Future multi-messenger detection rates of sGRBs, kilonovae and afterglows can be used for constraining the jet structure.

In this paper, we adopt an AT2017gfo-like model as our standard kilonova model to calculate the kilonova detectability of serendipitous and GW-triggered ToO observations. However, many theoretical works in the literature (e.g., Kasen et al. 2013, 2017; Kawaguchi et al. 2020, 2021; Darbha & Kasen 2020; Korobkin et al. 2021; Wollaeger et al. 2021) show that BNS kilonova should be diverse which may depend on the mass ratio of binary and the nature of the merger remnant. The possible energy injection from the merger remnant, e.g., due to spindown of a post-merger magnetar (Yu et al. 2013, 2018; Metzger & Piro 2014; Ai et al. 2018; Li et al. 2018; Ren et al. 2019)¹⁰ or fall-back accretion onto the post-merger BH (Rosswog 2007; Ma et al. 2018) could significantly increase the brightness of the kilonova. The diversity of kilonova and potential energy injection may affect on the final detection rate of kilonova, which will be studied in future work.

Software: POSSIS (Bulla 2019; Coughlin et al. 2020b); Matlab, <https://www.mathworks.com>; Python,

<https://www.python.org>; LALSuite, (LIGO Scientific Collaboration 2018)

ACKNOWLEDGMENTS

We thank the anonymous referees for constructive comments. We thank Xue-Feng Wu and Jiming Yu for valuable comments. The work of J.P.Z is partially supported by the National Science Foundation of China under Grant No. 11721303 and the National Basic Research Program of China under grant No. 2014CB845800. Y.P.Y is supported by National Natural Science Foundation of China grant No. 12003028, the National Key Research and Development Program of China (2022SKA0130101), and the China Manned Space Project (CMS-CSST-2021-B11). Z.J.C is supported by the National Natural Science Foundation of China (No. 11690023). H.G. is supported by the National Natural Science Foundation of China under Grant No. 11690024, 12021003, 11633001. Y.W.Y is supported by the National Natural Science Foundation of China under Grant No. 11822302, 11833003. L.S. is supported by the National Natural Science Foundation of China under Grant No. 11975027, and the Max Planck Partner Group Program funded by the Max Planck Society.

APPENDIX

A. AMPLITUDE SPECTRAL DENSITY

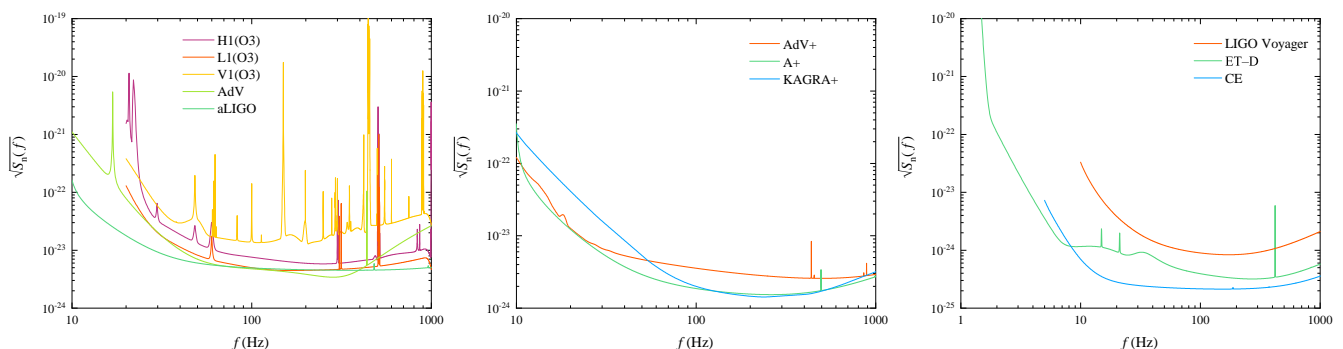


Figure 12. Left panel: the design sensitivity curves of 2nd generation GW detectors and O3 sensitivity curves. Middle panel: the design sensitivity curves of 2.5th generation GW detectors. Right panel: the design sensitivity curves of 3rd generation GW detectors.

¹⁰ The dissipation of wind from remnant magnetar (Zhang 2013) or interaction between the relativistic magnetar-driven ejecta and the circumstellar medium (Gao et al. 2013a; Liu et al. 2020) may also produce additional optical emission.

The ASD sensitivity curves of GW detectors used in our calculations are presented in Figure 12. For O3, we adopt the GW190814’s sensitivity curves¹¹ as the O3 sensitivity. The detector sensitivities during HLV (O4), PlusNetwork and LIGO Voyager era are adopted from the public data^{12,13}. The sensitivity curves of ET and CE used in this paper come from the official websites^{14,15}.

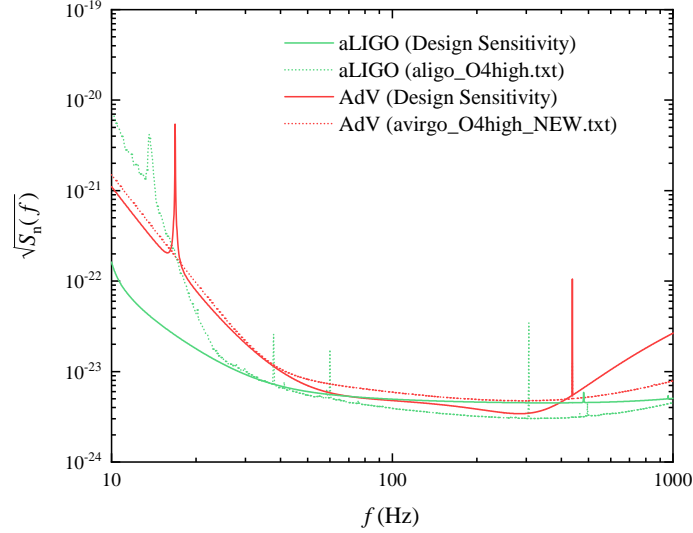


Figure 13. Design sensitivity curves (solid lines) and latest O4 sensitivity curves (dashed lines) of Advanced LIGO (red lines) and Advanced Virgo (green lines).

For 2nd generation detectors, we also compare their design sensitivity curves to the latest sensitivity curves released on April 6th, 2022¹⁶ in Figure 13.

REFERENCES

- Abbott, B. P., Abbott, R., Abbott, T. D., et al. 2017a, *PhRvL*, 119, 161101, doi: [10.1103/PhysRevLett.119.161101](https://doi.org/10.1103/PhysRevLett.119.161101)
- . 2017b, *ApJL*, 848, L13, doi: [10.3847/2041-8213/aa920c](https://doi.org/10.3847/2041-8213/aa920c)
- . 2017c, *ApJL*, 848, L12, doi: [10.3847/2041-8213/aa91c9](https://doi.org/10.3847/2041-8213/aa91c9)
- . 2019, *Physical Review X*, 9, 011001, doi: [10.1103/PhysRevX.9.011001](https://doi.org/10.1103/PhysRevX.9.011001)
- . 2020a, *Living Reviews in Relativity*, 23, 3, doi: [10.1007/s41114-020-00026-9](https://doi.org/10.1007/s41114-020-00026-9)
- . 2020b, *ApJL*, 892, L3, doi: [10.3847/2041-8213/ab75f5](https://doi.org/10.3847/2041-8213/ab75f5)
- Abbott, R., Abbott, T. D., Abraham, S., et al. 2021a, *ApJL*, 915, L5, doi: [10.3847/2041-8213/ac082e](https://doi.org/10.3847/2041-8213/ac082e)
- . 2021b, *ApJL*, 913, L7, doi: [10.3847/2041-8213/abe949](https://doi.org/10.3847/2041-8213/abe949)
- . 2021c, *Physical Review X*, 11, 021053, doi: [10.1103/PhysRevX.11.021053](https://doi.org/10.1103/PhysRevX.11.021053)
- Acerese, F., Agathos, M., Agatsuma, K., et al. 2015, *Classical and Quantum Gravity*, 32, 024001, doi: [10.1088/0264-9381/32/2/024001](https://doi.org/10.1088/0264-9381/32/2/024001)
- Adhikari, R. X., Arai, K., Brooks, A. F., et al. 2020, *Classical and Quantum Gravity*, 37, 165003, doi: [10.1088/1361-6382/ab9143](https://doi.org/10.1088/1361-6382/ab9143)
- Ai, S., Gao, H., Dai, Z.-G., et al. 2018, *ApJ*, 860, 57, doi: [10.3847/1538-4357/aac2b7](https://doi.org/10.3847/1538-4357/aac2b7)
- Alexander, K. D., Berger, E., Fong, W., et al. 2017, *ApJL*, 848, L21, doi: [10.3847/2041-8213/aa905d](https://doi.org/10.3847/2041-8213/aa905d)
- Almualla, M., Anand, S., Coughlin, M. W., et al. 2021, *MNRAS*, 504, 2822, doi: [10.1093/mnras/stab1090](https://doi.org/10.1093/mnras/stab1090)
- Andreoni, I., Ackley, K., Cooke, J., et al. 2017, *PASA*, 34, e069, doi: [10.1017/pasa.2017.65](https://doi.org/10.1017/pasa.2017.65)
- Andreoni, I., Coughlin, M. W., Almualla, M., et al. 2021a, arXiv e-prints, arXiv:2106.06820, <https://arxiv.org/abs/2106.06820>
- Andreoni, I., Coughlin, M. W., Kool, E. C., et al. 2021b, *ApJ*, 918, 63, doi: [10.3847/1538-4357/ac0bc7](https://doi.org/10.3847/1538-4357/ac0bc7)
- ¹¹ <https://dcc.ligo.org/P2000183/public>
- ¹² <https://dcc.ligo.org/LIGO-P1200087-v42/public>
- ¹³ <https://dcc.ligo.org/LIGO-T1500293/public>
- ¹⁴ <http://www.et-gw.eu/index.php/etsensitivities>
- ¹⁵ <https://dcc.cosmicexplorer.org/cgi-bin/DocDB/ShowDocument?docid=T2000017>
- ¹⁶ <https://dcc.ligo.org/LIGO-T2000012-v2/public>

- Arcavi, I., Hosseinzadeh, G., Howell, D. A., et al. 2017, *Nature*, 551, 64, doi: [10.1038/nature24291](https://doi.org/10.1038/nature24291)
- Ascenzi, S., Coughlin, M. W., Dietrich, T., et al. 2019, *MNRAS*, 486, 672, doi: [10.1093/mnras/stz891](https://doi.org/10.1093/mnras/stz891)
- Aso, Y., Michimura, Y., Somiya, K., et al. 2013, *PhRvD*, 88, 043007, doi: [10.1103/PhysRevD.88.043007](https://doi.org/10.1103/PhysRevD.88.043007)
- Barack, L., & Cutler, C. 2004, *PhRvD*, 69, 082005, doi: [10.1103/PhysRevD.69.082005](https://doi.org/10.1103/PhysRevD.69.082005)
- Bellm, E. C., Kulkarni, S. R., Graham, M. J., et al. 2019, *PASP*, 131, 018002, doi: [10.1088/1538-3873/aaecbe](https://doi.org/10.1088/1538-3873/aaecbe)
- Berger, E., Fong, W., & Chornock, R. 2013, *ApJL*, 774, L23, doi: [10.1088/2041-8205/774/2/L23](https://doi.org/10.1088/2041-8205/774/2/L23)
- Broekgaarden, F. S., Berger, E., Neijssel, C. J., et al. 2021, arXiv e-prints, arXiv:2103.02608. <https://arxiv.org/abs/2103.02608>
- Bulla, M. 2019, *MNRAS*, 489, 5037, doi: [10.1093/mnras/stz2495](https://doi.org/10.1093/mnras/stz2495)
- Chase, E. A., O'Connor, B., Fryer, C. L., et al. 2021, arXiv e-prints, arXiv:2105.12268. <https://arxiv.org/abs/2105.12268>
- Cheng, K. S., & Wang, J.-M. 1999, *ApJ*, 521, 502, doi: [10.1086/307572](https://doi.org/10.1086/307572)
- Chornock, R., Berger, E., Kasen, D., et al. 2017, *ApJL*, 848, L19, doi: [10.3847/2041-8213/aa905c](https://doi.org/10.3847/2041-8213/aa905c)
- Coughlin, M., Dietrich, T., Kawaguchi, K., et al. 2017, *ApJ*, 849, 12, doi: [10.3847/1538-4357/aa9114](https://doi.org/10.3847/1538-4357/aa9114)
- Coughlin, M. W., Dietrich, T., Antier, S., et al. 2020a, *MNRAS*, 497, 1181, doi: [10.1093/mnras/staa1925](https://doi.org/10.1093/mnras/staa1925)
- Coughlin, M. W., Antier, S., Dietrich, T., et al. 2020b, *Nature Communications*, 11, 4129, doi: [10.1038/s41467-020-17998-5](https://doi.org/10.1038/s41467-020-17998-5)
- Coulter, D. A., Foley, R. J., Kilpatrick, C. D., et al. 2017, *Science*, 358, 1556, doi: [10.1126/science.aap9811](https://doi.org/10.1126/science.aap9811)
- Covino, S., Wiersema, K., Fan, Y. Z., et al. 2017, *Nature Astronomy*, 1, 791, doi: [10.1038/s41550-017-0285-z](https://doi.org/10.1038/s41550-017-0285-z)
- Cowperthwaite, P. S., Villar, V. A., Scolnic, D. M., & Berger, E. 2019, *ApJ*, 874, 88, doi: [10.3847/1538-4357/ab07b6](https://doi.org/10.3847/1538-4357/ab07b6)
- Cowperthwaite, P. S., Berger, E., Villar, V. A., et al. 2017, *ApJL*, 848, L17, doi: [10.3847/2041-8213/aa8fc7](https://doi.org/10.3847/2041-8213/aa8fc7)
- Cutler, C., & Flanagan, E. E. 1994, *Physical Review D*, 49, 2658
- Darbha, S., & Kasen, D. 2020, *ApJ*, 897, 150, doi: [10.3847/1538-4357/ab9a34](https://doi.org/10.3847/1538-4357/ab9a34)
- D'Avanzo, P., Salvaterra, R., Bernardini, M. G., et al. 2014, *MNRAS*, 442, 2342, doi: [10.1093/mnras/stu994](https://doi.org/10.1093/mnras/stu994)
- D'Avanzo, P., Campana, S., Salafia, O. S., et al. 2018, *A&A*, 613, L1, doi: [10.1051/0004-6361/201832664](https://doi.org/10.1051/0004-6361/201832664)
- Díaz, M. C., Macri, L. M., Garcia Lambas, D., et al. 2017, *ApJL*, 848, L29, doi: [10.3847/2041-8213/aa9060](https://doi.org/10.3847/2041-8213/aa9060)
- Dietrich, T., Samajdar, A., Khan, S., et al. 2019, *PhRvD*, 100, 044003, doi: [10.1103/PhysRevD.100.044003](https://doi.org/10.1103/PhysRevD.100.044003)
- Dobie, D., Kaplan, D. L., Murphy, T., et al. 2018, *ApJL*, 858, L15, doi: [10.3847/2041-8213/aac105](https://doi.org/10.3847/2041-8213/aac105)
- Drout, M. R., Piro, A. L., Shappee, B. J., et al. 2017, *Science*, 358, 1570, doi: [10.1126/science.aaq0049](https://doi.org/10.1126/science.aaq0049)
- Drozda, P., Belczynski, K., O'Shaughnessy, R., Bulik, T., & Fryer, C. L. 2020, arXiv e-prints, arXiv:2009.06655. <https://arxiv.org/abs/2009.06655>
- Eichler, D., Livio, M., Piran, T., & Schramm, D. N. 1989, *Nature*, 340, 126, doi: [10.1038/340126a0](https://doi.org/10.1038/340126a0)
- Evans, P. A., Cenko, S. B., Kennea, J. A., et al. 2017, *Science*, 358, 1565, doi: [10.1126/science.aap9580](https://doi.org/10.1126/science.aap9580)
- Fan, Y.-Z., Yu, Y.-W., Xu, D., et al. 2013, *ApJL*, 779, L25, doi: [10.1088/2041-8205/779/2/L25](https://doi.org/10.1088/2041-8205/779/2/L25)
- Fong, W., Berger, E., Margutti, R., & Zauderer, B. A. 2015, *ApJ*, 815, 102, doi: [10.1088/0004-637X/815/2/102](https://doi.org/10.1088/0004-637X/815/2/102)
- Fong, W., Laskar, T., Rastinejad, J., et al. 2021, *ApJ*, 906, 127, doi: [10.3847/1538-4357/abc74a](https://doi.org/10.3847/1538-4357/abc74a)
- Fong, W.-f., Nugent, A. E., Dong, Y., et al. 2022, arXiv e-prints, arXiv:2206.01763. <https://arxiv.org/abs/2206.01763>
- Frostig, D., Biscoveanu, S., Mo, G., et al. 2021, arXiv e-prints, arXiv:2110.01622. <https://arxiv.org/abs/2110.01622>
- Gao, H., Ding, X., Wu, X.-F., Dai, Z.-G., & Zhang, B. 2015, *ApJ*, 807, 163, doi: [10.1088/0004-637X/807/2/163](https://doi.org/10.1088/0004-637X/807/2/163)
- Gao, H., Ding, X., Wu, X.-F., Zhang, B., & Dai, Z.-G. 2013a, *ApJ*, 771, 86, doi: [10.1088/0004-637X/771/2/86](https://doi.org/10.1088/0004-637X/771/2/86)
- Gao, H., Lei, W.-H., Zou, Y.-C., Wu, X.-F., & Zhang, B. 2013b, *NewAR*, 57, 141, doi: [10.1016/j.newar.2013.10.001](https://doi.org/10.1016/j.newar.2013.10.001)
- Gao, H., Zhang, B., & Lü, H.-J. 2016, *PhRvD*, 93, 044065, doi: [10.1103/PhysRevD.93.044065](https://doi.org/10.1103/PhysRevD.93.044065)
- Gao, H., Zhang, B., Lü, H.-J., & Li, Y. 2017, *ApJ*, 837, 50, doi: [10.3847/1538-4357/aa5be3](https://doi.org/10.3847/1538-4357/aa5be3)
- Gehrels, N., Chincarini, G., Giommi, P., et al. 2004, *ApJ*, 611, 1005, doi: [10.1086/422091](https://doi.org/10.1086/422091)
- Ghirlanda, G., Salafia, O. S., Paragi, Z., et al. 2019, *Science*, 363, 968, doi: [10.1126/science.aau8815](https://doi.org/10.1126/science.aau8815)
- Goldstein, A., Veres, P., Burns, E., et al. 2017, *ApJL*, 848, L14, doi: [10.3847/2041-8213/aa8f41](https://doi.org/10.3847/2041-8213/aa8f41)
- Gompertz, B. P., Levan, A. J., Tanvir, N. R., et al. 2018, *ApJ*, 860, 62, doi: [10.3847/1538-4357/aac206](https://doi.org/10.3847/1538-4357/aac206)
- Haggard, D., Nynka, M., Ruan, J. J., et al. 2017, *ApJL*, 848, L25, doi: [10.3847/2041-8213/aa8ede](https://doi.org/10.3847/2041-8213/aa8ede)
- Hallinan, G., Corsi, A., Mooley, K. P., et al. 2017, *Science*, 358, 1579, doi: [10.1126/science.aap9855](https://doi.org/10.1126/science.aap9855)
- Hao, J.-M., & Yuan, Y.-F. 2013, *A&A*, 558, A22, doi: [10.1051/0004-6361/201321471](https://doi.org/10.1051/0004-6361/201321471)

- Harry, G. M., & LIGO Scientific Collaboration. 2010, *Classical and Quantum Gravity*, 27, 084006, doi: [10.1088/0264-9381/27/8/084006](https://doi.org/10.1088/0264-9381/27/8/084006)
- Hu, L., Wu, X., Andreoni, I., et al. 2017, *Science Bulletin*, 62, 1433, doi: [10.1016/j.scib.2017.10.006](https://doi.org/10.1016/j.scib.2017.10.006)
- Hu, R.-C., Zhu, J.-P., Qin, Y., et al. 2022, *ApJ*, 928, 163, doi: [10.3847/1538-4357/ac573f](https://doi.org/10.3847/1538-4357/ac573f)
- Jin, Z.-P., Covino, S., Liao, N.-H., et al. 2020, *Nature Astronomy*, 4, 77, doi: [10.1038/s41550-019-0892-y](https://doi.org/10.1038/s41550-019-0892-y)
- Jin, Z.-P., Li, X., Cano, Z., et al. 2015, *ApJL*, 811, L22, doi: [10.1088/2041-8205/811/2/L22](https://doi.org/10.1088/2041-8205/811/2/L22)
- Jin, Z.-P., Hotokezaka, K., Li, X., et al. 2016, *Nature Communications*, 7, 12898, doi: [10.1038/ncomms12898](https://doi.org/10.1038/ncomms12898)
- Kagra Collaboration, Akutsu, T., Ando, M., et al. 2019, *Nature Astronomy*, 3, 35, doi: [10.1038/s41550-018-0658-y](https://doi.org/10.1038/s41550-018-0658-y)
- Kang, Y., Liu, C., & Shao, L. 2022, *Mon. Not. Roy. Astron. Soc.*, 515, 739, doi: [10.1093/mnras/stac1738](https://doi.org/10.1093/mnras/stac1738)
- Kasen, D., Badnell, N. R., & Barnes, J. 2013, *ApJ*, 774, 25, doi: [10.1088/0004-637X/774/1/25](https://doi.org/10.1088/0004-637X/774/1/25)
- Kasen, D., Metzger, B., Barnes, J., Quataert, E., & Ramirez-Ruiz, E. 2017, *Nature*, 551, 80, doi: [10.1038/nature24453](https://doi.org/10.1038/nature24453)
- Kasliwal, M. M., Nakar, E., Singer, L. P., et al. 2017, *Science*, 358, 1559, doi: [10.1126/science.aap9455](https://doi.org/10.1126/science.aap9455)
- Kasliwal, M. M., Anand, S., Ahumada, T., et al. 2020, *ApJ*, 905, 145, doi: [10.3847/1538-4357/abc335](https://doi.org/10.3847/1538-4357/abc335)
- Kawaguchi, K., Fujibayashi, S., Shibata, M., Tanaka, M., & Wanajo, S. 2021, *ApJ*, 913, 100, doi: [10.3847/1538-4357/abf3bc](https://doi.org/10.3847/1538-4357/abf3bc)
- Kawaguchi, K., Shibata, M., & Tanaka, M. 2020, *ApJ*, 889, 171, doi: [10.3847/1538-4357/ab61f6](https://doi.org/10.3847/1538-4357/ab61f6)
- Kilpatrick, C. D., Foley, R. J., Kasen, D., et al. 2017, *Science*, 358, 1583, doi: [10.1126/science.aaq0073](https://doi.org/10.1126/science.aaq0073)
- Kiziltan, B., Kottas, A., De Yoreo, M., & Thorsett, S. E. 2013, *ApJ*, 778, 66, doi: [10.1088/0004-637X/778/1/66](https://doi.org/10.1088/0004-637X/778/1/66)
- Korobkin, O., Wollaeger, R. T., Fryer, C. L., et al. 2021, *ApJ*, 910, 116, doi: [10.3847/1538-4357/abe1b5](https://doi.org/10.3847/1538-4357/abe1b5)
- Lattimer, J. M. 2012, *Annual Review of Nuclear and Particle Science*, 62, 485, doi: [10.1146/annurev-nucl-102711-095018](https://doi.org/10.1146/annurev-nucl-102711-095018)
- Lazzati, D., Perna, R., Morsony, B. J., et al. 2018, *PhRvL*, 120, 241103, doi: [10.1103/PhysRevLett.120.241103](https://doi.org/10.1103/PhysRevLett.120.241103)
- Lei, L., Li, J., Wu, J., Jiang, S., & Chen, B. 2021, *Astronomical Research & Technology*, 18, L18, doi: [10.14005/j.cnki.issn1672-7673.20200713.001](https://doi.org/10.14005/j.cnki.issn1672-7673.20200713.001)
- Li, L.-X., & Paczyński, B. 1998, *ApJL*, 507, L59, doi: [10.1086/311680](https://doi.org/10.1086/311680)
- Li, S.-Z., Liu, L.-D., Yu, Y.-W., & Zhang, B. 2018, *ApJL*, 861, L12, doi: [10.3847/2041-8213/aace61](https://doi.org/10.3847/2041-8213/aace61)
- Lien, A., Sakamoto, T., Gehrels, N., et al. 2014, *ApJ*, 783, 24, doi: [10.1088/0004-637X/783/1/24](https://doi.org/10.1088/0004-637X/783/1/24)
- LIGO Scientific Collaboration. 2018, LIGO Algorithm Library - LALSuite, free software (GPL), doi: [10.7935/GT1W-FZ16](https://doi.org/10.7935/GT1W-FZ16)
- LIGO Scientific Collaboration, Aasi, J., Abbott, B. P., et al. 2015, *Classical and Quantum Gravity*, 32, 074001, doi: [10.1088/0264-9381/32/7/074001](https://doi.org/10.1088/0264-9381/32/7/074001)
- Lipunov, V. M., Gorbvskoy, E., Kornilov, V. G., et al. 2017, *ApJL*, 850, L1, doi: [10.3847/2041-8213/aa92c0](https://doi.org/10.3847/2041-8213/aa92c0)
- Liu, C., Kang, Y., & Shao, L. 2022, *Astrophys. J.*, 934, 84, doi: [10.3847/1538-4357/ac7a39](https://doi.org/10.3847/1538-4357/ac7a39)
- Liu, C., & Shao, L. 2022, *ApJ*, 926, 158, doi: [10.3847/1538-4357/ac3cbf](https://doi.org/10.3847/1538-4357/ac3cbf)
- Liu, J., Soria, R., Wu, X.-F., Wu, H., & Shang, Z. 2021, *An. Acad. Bras. Ciênc. vol.93 supl.1*, 93, 20200628, doi: [10.1590/0001-3765202120200628](https://doi.org/10.1590/0001-3765202120200628)
- Liu, L.-D., Gao, H., & Zhang, B. 2020, *ApJ*, 890, 102, doi: [10.3847/1538-4357/ab6b24](https://doi.org/10.3847/1538-4357/ab6b24)
- LSST Science Collaboration, Abell, P. A., Allison, J., et al. 2009, arXiv e-prints, arXiv:0912.0201. <https://arxiv.org/abs/0912.0201>
- Lyman, J. D., Lamb, G. P., Levan, A. J., et al. 2018, *Nature Astronomy*, 2, 751, doi: [10.1038/s41550-018-0511-3](https://doi.org/10.1038/s41550-018-0511-3)
- Ma, S.-B., Lei, W.-H., Gao, H., et al. 2018, *ApJL*, 852, L5, doi: [10.3847/2041-8213/aaa0cd](https://doi.org/10.3847/2041-8213/aaa0cd)
- Ma, S.-B., Xie, W., Liao, B., et al. 2021, *ApJ*, 911, 97, doi: [10.3847/1538-4357/abe71b](https://doi.org/10.3847/1538-4357/abe71b)
- Maggiore, M., Van Den Broeck, C., Bartolo, N., et al. 2020, *JCAP*, 2020, 050, doi: [10.1088/1475-7516/2020/03/050](https://doi.org/10.1088/1475-7516/2020/03/050)
- Mandel, I., & Broekgaarden, F. S. 2021, arXiv e-prints, arXiv:2107.14239. <https://arxiv.org/abs/2107.14239>
- Margutti, R., Berger, E., Fong, W., et al. 2017, *ApJL*, 848, L20, doi: [10.3847/2041-8213/aa9057](https://doi.org/10.3847/2041-8213/aa9057)
- Masci, F. J., Laher, R. R., Rusholme, B., et al. 2019, *PASP*, 131, 018003, doi: [10.1088/1538-3873/aae8ac](https://doi.org/10.1088/1538-3873/aae8ac)
- McCully, C., Hiramatsu, D., Howell, D. A., et al. 2017, *ApJL*, 848, L32, doi: [10.3847/2041-8213/aa9111](https://doi.org/10.3847/2041-8213/aa9111)
- McKernan, B., Ford, K. E. S., & O'Shaughnessy, R. 2020, *MNRAS*, 498, 4088, doi: [10.1093/mnras/staa2681](https://doi.org/10.1093/mnras/staa2681)
- Meegan, C., Lichti, G., Bhat, P. N., et al. 2009, *ApJ*, 702, 791, doi: [10.1088/0004-637X/702/1/791](https://doi.org/10.1088/0004-637X/702/1/791)
- Meszáros, P., & Rees, M. J. 1993, *ApJ*, 405, 278, doi: [10.1086/172360](https://doi.org/10.1086/172360)
- Mészáros, P., & Rees, M. J. 1997, *ApJ*, 476, 232, doi: [10.1086/303625](https://doi.org/10.1086/303625)
- Metzger, B. D., & Berger, E. 2012, *ApJ*, 746, 48, doi: [10.1088/0004-637X/746/1/48](https://doi.org/10.1088/0004-637X/746/1/48)
- Metzger, B. D., & Piro, A. L. 2014, *MNRAS*, 439, 3916, doi: [10.1093/mnras/stu247](https://doi.org/10.1093/mnras/stu247)

- Metzger, B. D., Martínez-Pinedo, G., Darbha, S., et al. 2010, *MNRAS*, 406, 2650, doi: [10.1111/j.1365-2966.2010.16864.x](https://doi.org/10.1111/j.1365-2966.2010.16864.x)
- Michimura, Y., Komori, K., Enomoto, Y., et al. 2020, *PhRvD*, 102, 022008, doi: [10.1103/PhysRevD.102.022008](https://doi.org/10.1103/PhysRevD.102.022008)
- Miller, J., Barsotti, L., Vitale, S., et al. 2015, *PhRvD*, 91, 062005, doi: [10.1103/PhysRevD.91.062005](https://doi.org/10.1103/PhysRevD.91.062005)
- Mohite, S. R., Rajkumar, P., Anand, S., et al. 2021, arXiv e-prints, arXiv:2107.07129. <https://arxiv.org/abs/2107.07129>
- Nakar, E., Gal-Yam, A., & Fox, D. B. 2006, *ApJ*, 650, 281, doi: [10.1086/505855](https://doi.org/10.1086/505855)
- Narayan, R., Paczynski, B., & Piran, T. 1992, *ApJL*, 395, L83, doi: [10.1086/186493](https://doi.org/10.1086/186493)
- Nicholl, M., Berger, E., Kasen, D., et al. 2017, *ApJL*, 848, L18, doi: [10.3847/2041-8213/aa9029](https://doi.org/10.3847/2041-8213/aa9029)
- Nugent, A. E., Fong, W.-f., Dong, Y., et al. 2022, arXiv e-prints, arXiv:2206.01764. <https://arxiv.org/abs/2206.01764>
- O'Connor, B., Troja, E., Dichiara, S., et al. 2022, *MNRAS*, 515, 4890, doi: [10.1093/mnras/stac1982](https://doi.org/10.1093/mnras/stac1982)
- Paczynski, B. 1986, *ApJL*, 308, L43, doi: [10.1086/184740](https://doi.org/10.1086/184740)
- . 1991, *AcA*, 41, 257
- Paczynski, B., & Rhoads, J. E. 1993, *ApJL*, 418, L5, doi: [10.1086/187102](https://doi.org/10.1086/187102)
- Perna, R., Lazzati, D., & Cantiello, M. 2021, *ApJL*, 906, L7, doi: [10.3847/2041-8213/abd319](https://doi.org/10.3847/2041-8213/abd319)
- Petrov, P., Singer, L. P., Coughlin, M. W., et al. 2022, *ApJ*, 924, 54, doi: [10.3847/1538-4357/ac366d](https://doi.org/10.3847/1538-4357/ac366d)
- Pian, E., D'Avanzo, P., Benetti, S., et al. 2017, *Nature*, 551, 67, doi: [10.1038/nature24298](https://doi.org/10.1038/nature24298)
- Piro, L., Troja, E., Zhang, B., et al. 2019, *MNRAS*, 483, 1912, doi: [10.1093/mnras/sty3047](https://doi.org/10.1093/mnras/sty3047)
- Planck Collaboration, Ade, P. A. R., Aghanim, N., et al. 2016, *A&A*, 594, A13, doi: [10.1051/0004-6361/201525830](https://doi.org/10.1051/0004-6361/201525830)
- Punturo, M., Abernathy, M., Acernese, F., et al. 2010a, *Classical and Quantum Gravity*, 27, 194002, doi: [10.1088/0264-9381/27/19/194002](https://doi.org/10.1088/0264-9381/27/19/194002)
- . 2010b, *Classical and Quantum Gravity*, 27, 084007, doi: [10.1088/0264-9381/27/8/084007](https://doi.org/10.1088/0264-9381/27/8/084007)
- Rastinejad, J. C., Gompertz, B. P., Levan, A. J., et al. 2022, arXiv e-prints, arXiv:2204.10864. <https://arxiv.org/abs/2204.10864>
- Rees, M. J., & Meszaros, P. 1992, *MNRAS*, 258, 41, doi: [10.1093/mnras/258.1.41P](https://doi.org/10.1093/mnras/258.1.41P)
- Reitze, D., Adhikari, R. X., Ballmer, S., et al. 2019, in *Bulletin of the American Astronomical Society*, Vol. 51, 35. <https://arxiv.org/abs/1907.04833>
- Ren, J., Lin, D.-B., Zhang, L.-L., et al. 2019, *ApJ*, 885, 60, doi: [10.3847/1538-4357/ab4188](https://doi.org/10.3847/1538-4357/ab4188)
- Rossi, A., Stratta, G., Maiorano, E., et al. 2020, *MNRAS*, 493, 3379, doi: [10.1093/mnras/staa479](https://doi.org/10.1093/mnras/staa479)
- Rosswog, S. 2007, *MNRAS*, 376, L48, doi: [10.1111/j.1745-3933.2007.00284.x](https://doi.org/10.1111/j.1745-3933.2007.00284.x)
- Rosswog, S., Feindt, U., Korobkin, O., et al. 2017, *Classical and Quantum Gravity*, 34, 104001, doi: [10.1088/1361-6382/aa68a9](https://doi.org/10.1088/1361-6382/aa68a9)
- Sagués Carracedo, A., Bulla, M., Feindt, U., & Goobar, A. 2021, *MNRAS*, 504, 1294, doi: [10.1093/mnras/stab872](https://doi.org/10.1093/mnras/stab872)
- Sari, R., Piran, T., & Narayan, R. 1998, *ApJL*, 497, L17, doi: [10.1086/311269](https://doi.org/10.1086/311269)
- Sarin, N., Lasky, P. D., Vivanco, F. H., et al. 2022, *PhRvD*, 105, 083004, doi: [10.1103/PhysRevD.105.083004](https://doi.org/10.1103/PhysRevD.105.083004)
- Savchenko, V., Ferrigno, C., Kuulkers, E., et al. 2017, *ApJL*, 848, L15, doi: [10.3847/2041-8213/aa8f94](https://doi.org/10.3847/2041-8213/aa8f94)
- Scolnic, D., Kessler, R., Brout, D., et al. 2018, *ApJL*, 852, L3, doi: [10.3847/2041-8213/aa9d82](https://doi.org/10.3847/2041-8213/aa9d82)
- Setzer, C. N., Biswas, R., Peiris, H. V., et al. 2019, *MNRAS*, 485, 4260, doi: [10.1093/mnras/stz506](https://doi.org/10.1093/mnras/stz506)
- Shappee, B. J., Simon, J. D., Drout, M. R., et al. 2017, *Science*, 358, 1574, doi: [10.1126/science.aaq0186](https://doi.org/10.1126/science.aaq0186)
- Shi, D.-D., Zheng, X.-Z., Zhao, H.-B., et al. 2018, *ACTA ASTRONOMICA SINICA*, 59, 1, doi: [10.15940/j.cnki.0001-5245.2018.03.001](https://doi.org/10.15940/j.cnki.0001-5245.2018.03.001)
- Singer, L. P., & Price, L. R. 2016, *PhRvD*, 93, 024013, doi: [10.1103/PhysRevD.93.024013](https://doi.org/10.1103/PhysRevD.93.024013)
- Singh, K. P., Tandon, S. N., Agrawal, P. C., et al. 2014, in *Society of Photo-Optical Instrumentation Engineers (SPIE) Conference Series*, Vol. 9144, *Space Telescopes and Instrumentation 2014: Ultraviolet to Gamma Ray*, ed. T. Takahashi, J.-W. A. den Herder, & M. Bautz, 91441S, doi: [10.1117/12.2062667](https://doi.org/10.1117/12.2062667)
- Smartt, S. J., Chen, T. W., Jerkstrand, A., et al. 2017, *Nature*, 551, 75, doi: [10.1038/nature24303](https://doi.org/10.1038/nature24303)
- Soares-Santos, M., Holz, D. E., Annis, J., et al. 2017, *ApJL*, 848, L16, doi: [10.3847/2041-8213/aa9059](https://doi.org/10.3847/2041-8213/aa9059)
- Song, H.-R., Ai, S.-K., Wang, M.-H., et al. 2019, *ApJL*, 881, L40, doi: [10.3847/2041-8213/ab3921](https://doi.org/10.3847/2041-8213/ab3921)
- Sun, H., Zhang, B., & Li, Z. 2015, *ApJ*, 812, 33, doi: [10.1088/0004-637X/812/1/33](https://doi.org/10.1088/0004-637X/812/1/33)
- Tan, W.-W., & Yu, Y.-W. 2020, *ApJ*, 902, 83, doi: [10.3847/1538-4357/abb404](https://doi.org/10.3847/1538-4357/abb404)
- Tanvir, N. R., Levan, A. J., Fruchter, A. S., et al. 2013, *Nature*, 500, 547, doi: [10.1038/nature12505](https://doi.org/10.1038/nature12505)
- Tanvir, N. R., Levan, A. J., González-Fernández, C., et al. 2017, *ApJL*, 848, L27, doi: [10.3847/2041-8213/aa90b6](https://doi.org/10.3847/2041-8213/aa90b6)
- Thrane, E., & Talbot, C. 2019, *Publications of the Astronomical Society of Australia*, 36
- Troja, E., Piro, L., van Eerten, H., et al. 2017, *Nature*, 551, 71, doi: [10.1038/nature24290](https://doi.org/10.1038/nature24290)

- Troja, E., Piro, L., Ryan, G., et al. 2018, *MNRAS*, 478, L18, doi: [10.1093/mnras/sly061](https://doi.org/10.1093/mnras/sly061)
- Troja, E., van Eerten, H., Zhang, B., et al. 2020, *MNRAS*, 498, 5643, doi: [10.1093/mnras/staa2626](https://doi.org/10.1093/mnras/staa2626)
- Troja, E., Fryer, C. L., O'Connor, B., et al. 2022, arXiv e-prints, arXiv:2209.03363. <https://arxiv.org/abs/2209.03363>
- Typel, S., Röpke, G., Klähn, T., Blaschke, D., & Wolter, H. H. 2010, *PhRvC*, 81, 015803, doi: [10.1103/PhysRevC.81.015803](https://doi.org/10.1103/PhysRevC.81.015803)
- Utsumi, Y., Tanaka, M., Tominaga, N., et al. 2017, *PASJ*, 69, 101, doi: [10.1093/pasj/psx118](https://doi.org/10.1093/pasj/psx118)
- Valenti, S., Sand, D. J., Yang, S., et al. 2017, *ApJL*, 848, L24, doi: [10.3847/2041-8213/aa8edf](https://doi.org/10.3847/2041-8213/aa8edf)
- Villar, V. A., Guillochon, J., Berger, E., et al. 2017, *ApJL*, 851, L21, doi: [10.3847/2041-8213/aa9c84](https://doi.org/10.3847/2041-8213/aa9c84)
- Virgili, F. J., Zhang, B., O'Brien, P., & Troja, E. 2011, *ApJ*, 727, 109, doi: [10.1088/0004-637X/727/2/109](https://doi.org/10.1088/0004-637X/727/2/109)
- Vitale, S., & Evans, M. 2017, *PhRvD*, 95, 064052, doi: [10.1103/PhysRevD.95.064052](https://doi.org/10.1103/PhysRevD.95.064052)
- Vitale, S., & Whittle, C. 2018, *PhRvD*, 98, 024029, doi: [10.1103/PhysRevD.98.024029](https://doi.org/10.1103/PhysRevD.98.024029)
- Wanderman, D., & Piran, T. 2015, *MNRAS*, 448, 3026, doi: [10.1093/mnras/stv123](https://doi.org/10.1093/mnras/stv123)
- Wollaeger, R. T., Fryer, C. L., Chase, E. A., et al. 2021, *ApJ*, 918, 10, doi: [10.3847/1538-4357/ac0d03](https://doi.org/10.3847/1538-4357/ac0d03)
- Wu, G.-L., Yu, Y.-W., & Zhu, J.-P. 2021, arXiv e-prints, arXiv:2108.01349. <https://arxiv.org/abs/2108.01349>
- Xie, X., Zrake, J., & MacFadyen, A. 2018, *ApJ*, 863, 58, doi: [10.3847/1538-4357/aac9c](https://doi.org/10.3847/1538-4357/aac9c)
- Yang, B., Jin, Z.-P., Li, X., et al. 2015, *Nature Communications*, 6, 7323, doi: [10.1038/ncomms8323](https://doi.org/10.1038/ncomms8323)
- Yang, F., Wang, W., Wei, X., et al. 2022a, *Research in Astronomy and Astrophysics*, 22, 055005, doi: [10.1088/1674-4527/ac5801](https://doi.org/10.1088/1674-4527/ac5801)
- Yang, J., Ai, S., Zhang, B.-B., et al. 2022b, arXiv e-prints, arXiv:2204.12771. <https://arxiv.org/abs/2204.12771>
- Yu, J., Song, H., Ai, S., et al. 2021, *ApJ*, 916, 54, doi: [10.3847/1538-4357/ac0628](https://doi.org/10.3847/1538-4357/ac0628)
- Yu, Y.-W., Liu, L.-D., & Dai, Z.-G. 2018, *ApJ*, 861, 114, doi: [10.3847/1538-4357/aac6e5](https://doi.org/10.3847/1538-4357/aac6e5)
- Yu, Y.-W., Zhang, B., & Gao, H. 2013, *ApJL*, 776, L40, doi: [10.1088/2041-8205/776/2/L40](https://doi.org/10.1088/2041-8205/776/2/L40)
- Yuan, Y., Lü, H.-J., Yuan, H.-Y., et al. 2021, *ApJ*, 912, 14, doi: [10.3847/1538-4357/abedb1](https://doi.org/10.3847/1538-4357/abedb1)
- Zappa, F., Bernuzzi, S., Pannarale, F., Mapelli, M., & Giacobbo, N. 2019, *PhRvL*, 123, 041102, doi: [10.1103/PhysRevLett.123.041102](https://doi.org/10.1103/PhysRevLett.123.041102)
- Zevin, M., Nugent, A. E., Adhikari, S., et al. 2022, arXiv e-prints, arXiv:2206.02814. <https://arxiv.org/abs/2206.02814>
- Zhang, B. 2013, *ApJL*, 763, L22, doi: [10.1088/2041-8205/763/1/L22](https://doi.org/10.1088/2041-8205/763/1/L22)
- . 2018, *The Physics of Gamma-Ray Bursts*, doi: [10.1017/9781139226530](https://doi.org/10.1017/9781139226530)
- Zhang, B., & Mészáros, P. 2002, *ApJ*, 571, 876, doi: [10.1086/339981](https://doi.org/10.1086/339981)
- Zhang, B. B., Zhang, B., Sun, H., et al. 2018a, *Nature Communications*, 9, 447, doi: [10.1038/s41467-018-02847-3](https://doi.org/10.1038/s41467-018-02847-3)
- Zhang, D.-L., Li, X.-Q., Xiong, S.-L., et al. 2018b, arXiv e-prints, arXiv:1804.04499. <https://arxiv.org/abs/1804.04499>
- Zhu, J.-P., Wang, K., & Zhang, B. 2021a, *ApJL*, 917, L28, doi: [10.3847/2041-8213/ac1a17](https://doi.org/10.3847/2041-8213/ac1a17)
- Zhu, J.-P., Wang, K., Zhang, B., et al. 2021b, *ApJL*, 911, L19, doi: [10.3847/2041-8213/abf2c3](https://doi.org/10.3847/2041-8213/abf2c3)
- Zhu, J.-P., Wang, X. I., Sun, H., et al. 2022a, *ApJL*, 936, L10, doi: [10.3847/2041-8213/ac85ad](https://doi.org/10.3847/2041-8213/ac85ad)
- Zhu, J.-P., Wu, S., Qin, Y., et al. 2022b, *ApJ*, 928, 167, doi: [10.3847/1538-4357/ac540c](https://doi.org/10.3847/1538-4357/ac540c)
- Zhu, J.-P., Wu, S., Yang, Y.-P., et al. 2021c, *ApJ*, 921, 156, doi: [10.3847/1538-4357/ac19a7](https://doi.org/10.3847/1538-4357/ac19a7)
- Zhu, J.-P., Yang, Y.-P., Liu, L.-D., et al. 2020, *ApJ*, 897, 20, doi: [10.3847/1538-4357/ab93bf](https://doi.org/10.3847/1538-4357/ab93bf)
- Zhu, J.-P., Yang, Y.-P., Zhang, B., Gao, H., & Yu, Y.-W. 2022c, *ApJ*, 938, 147, doi: [10.3847/1538-4357/ac8e60](https://doi.org/10.3847/1538-4357/ac8e60)
- Zhu, J.-P., Zhang, B., Yu, Y.-W., & Gao, H. 2021d, *ApJL*, 906, L11, doi: [10.3847/2041-8213/abd412](https://doi.org/10.3847/2041-8213/abd412)
- Zhu, J.-P., Wu, S., Yang, Y.-P., et al. 2021e, *ApJ*, 917, 24, doi: [10.3847/1538-4357/abfe5e](https://doi.org/10.3847/1538-4357/abfe5e)